
SOLEIL
SYNCHROTRON
Light!
Jean Daillant
Strasbourg 07/07/2015
INTERNATIONAL
YEAR OF LIGHT
2015

Synchrotron radiation

Radiation from a Moving Charge

Accelerated charge: Liénard, L'Eclairage Electrique, 1898

$$\mathbf{B}(\mathbf{r},t) = -\frac{q}{4\pi\epsilon_0 c^3 R}\mathbf{n}\times\mathbf{a}$$

$$\mathbf{E}(\mathbf{r},t) = \frac{q}{4\pi\epsilon_0 c^2 R}\mathbf{n}\times\mathbf{n}\times\mathbf{a}$$

$$\mathbf{S}.\mathbf{n} = \frac{q^2}{16\pi^2\epsilon_0 c^5}\frac{1}{R^2}\left|\mathbf{n}\times\mathbf{n}\times a]\right|^2$$

$$P = \frac{e^2}{6\pi\epsilon_0 c^3}\left|\mathbf{a}\right|^2$$

Larmor's formula

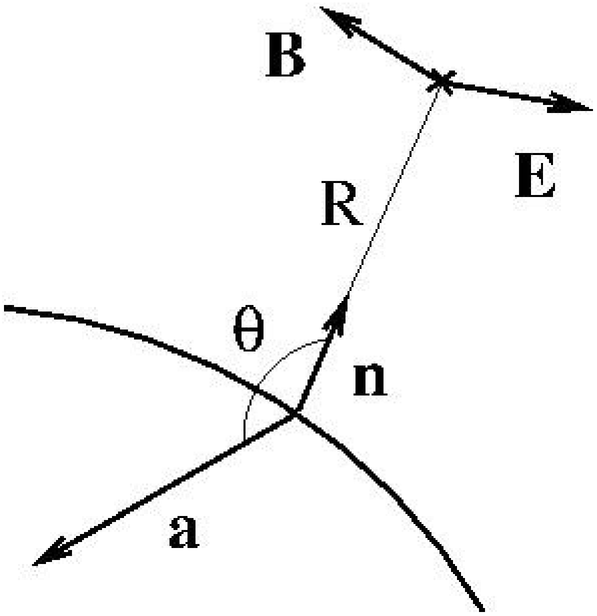

Relativistic Effects (I)

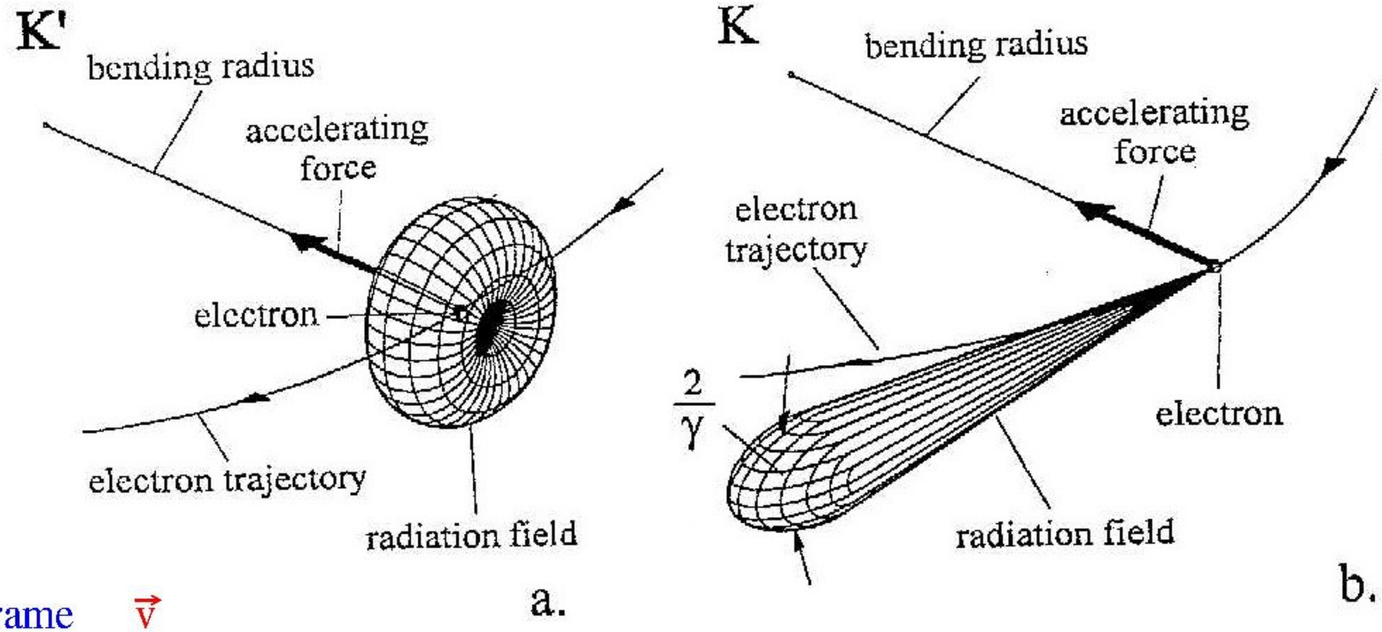

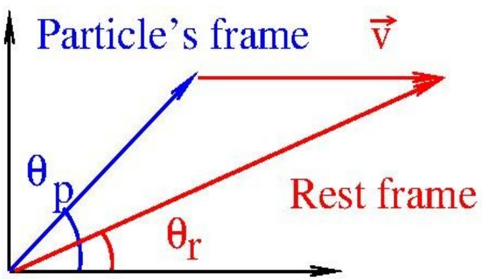

- Lorentz transform

$$x'=\gamma(x-vt);\gamma=1/\sqrt{1-v^2/c^2}$$

- Emission in a cone $1/\Upsilon$ with $\Upsilon=E/m_0c^2$
- m_0c^2=511keV ; for E=2.75GeV, Υ=5382
- $1/\Upsilon$ = 0.186mrad = 0.01°
- Polarization

Relativistic effects (II)

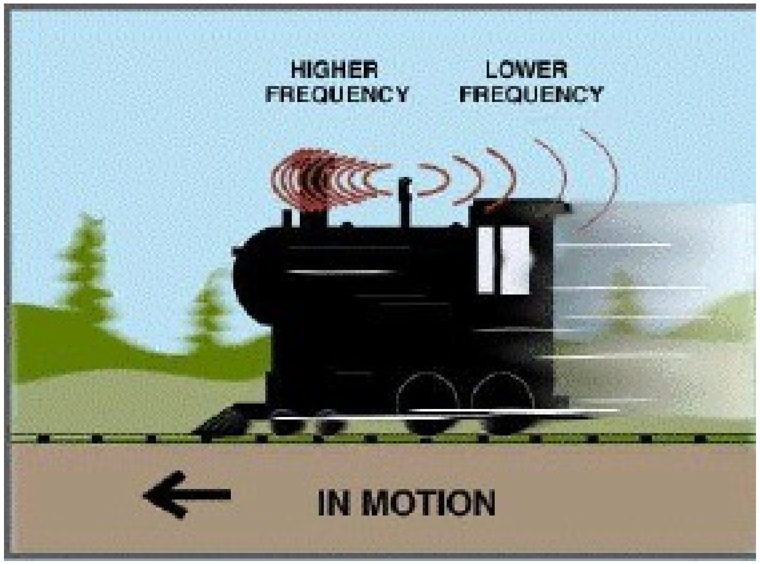

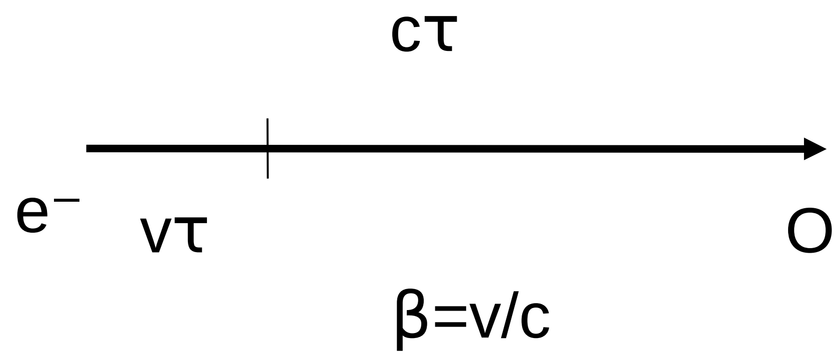

- Doppler effect
- Dilation of time

$$\lambda=(1-\beta)\lambda_0=\frac{1-\beta^2}{1+\beta}\lambda_0=\frac{\lambda_0}{2\gamma^2}$$

- X-rays !

Liénard-Wiechert Potentials

$$\mathbf{B}(\mathbf{r},t) = -\frac{\mu_0 q}{4\pi}\left[\frac{c\mathbf{n}\times\beta}{\gamma^2 R^2(1-\beta.\mathbf{n})^3} + \frac{\mathbf{n}\times[\dot{\beta}+\mathbf{n}\times(\beta\times\dot{\beta})]}{R(1-\beta.\mathbf{n})^3}\right]$$

$$\mathbf{E}(\mathbf{r},t) = \frac{q}{4\pi\epsilon_0}\left[\frac{\mathbf{n}-\beta}{\gamma^2 R^2(1-\beta.\mathbf{n})^3} + \frac{\mathbf{n}\times[(\mathbf{n}-\beta)\times\dot{\beta}]}{cR(1-\beta.\mathbf{n})^3}\right]$$

$$\mathbf{S}.\mathbf{n} = \frac{q^2}{16\pi^2\epsilon_0 c}\frac{1}{R^2}\left|\frac{\mathbf{n}\times[(\mathbf{n}-\beta)\times\dot{\beta}]}{(1-\beta.\mathbf{n})^3}\right|^2$$

$$P = \frac{e^2}{6\pi\epsilon_0 c}\gamma^6\left[\left|\dot{\beta}\right|^2 - \left|\beta\times\dot{\beta}\right|^2\right]$$

$$\beta = \mathbf{v}/c$$

Magnet

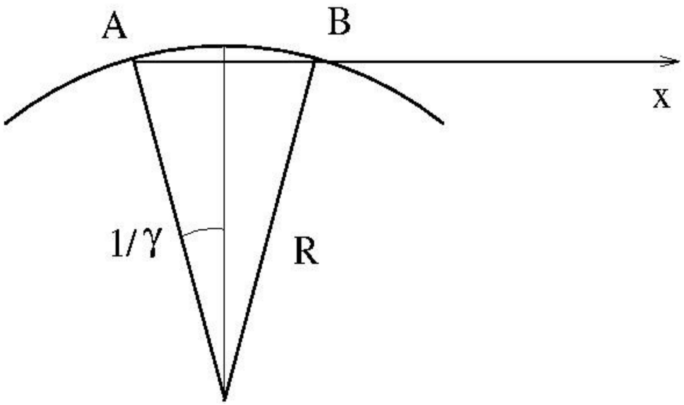

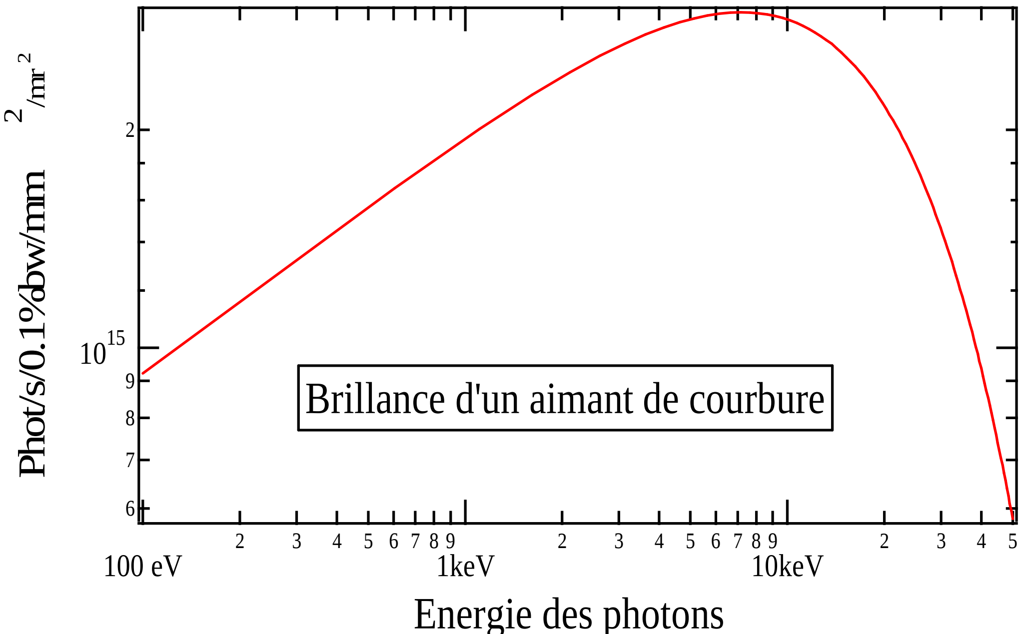

- Velocity ⊥ acceleration
- Emission during $\Delta t = 2\rho/\gamma v$

When e⁻ reaches B, light has already travelled $\Delta x = 2\rho c/\gamma v$

- Pulse duration is hence :

$$\frac{2\rho c}{\gamma v} - 2\rho \sin(1/\gamma) \approx \frac{4\rho}{3\gamma^3 c}$$

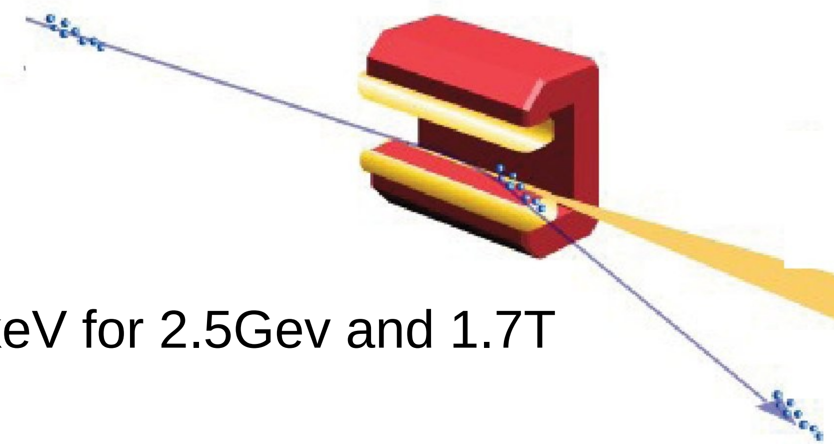

- Critical Energy : $E_c = \frac{3\gamma^3 \hbar c}{2\rho}$ = 8.6keV for 2.5Gev and 1.7T
- $T_0 = 1/(2\pi Rc)$ = 0.3µs for R=56m

Undulator

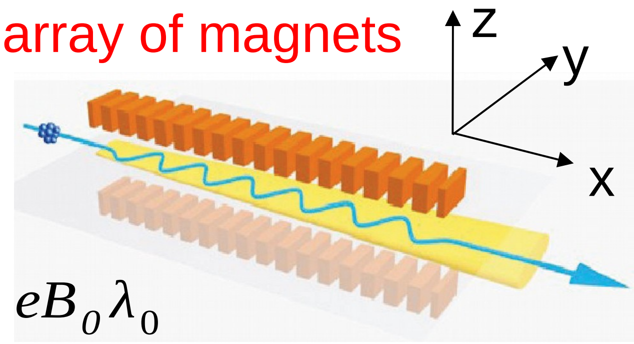

- Magnetic field $B_z = B_0 \cos\left(2\pi x/\lambda_0\right)$
- Lorentz force : $\gamma m_0 \frac{dv_y}{dt} \approx e v_0 B_0 \cos\left(2\pi x/\lambda\right)$
- Trajectory : $y = -\frac{K\lambda_0}{2\pi\gamma}\cos\left(2\pi x/\lambda_0\right)$ with $K = \frac{eB_0\lambda_0}{2\pi m_0 c}$
- K, undulator strength ; with E=2.75Gev, B_0=1T, λ_0=20mm, K=1.9, the maximum deviation of the e^- beam is 1.1µm
- Over λ_0, the e^- will travel an extra distance $\delta L = \int_0^{\lambda_0}\left(\sqrt{1+\left(\frac{dy}{dx}\right)^2} - 1\right)dx = \frac{K^2\lambda_0}{4\gamma^2}$
- The time needed by the e^- to cover a period will be larger than the time needed by the photon by $\delta t = \frac{\lambda_0 + \delta L}{v_0} - \frac{\lambda_0}{c} = \frac{\lambda_0}{2\gamma^2 c}\left(1 + \frac{K^2}{2}\right)$
- e^- with δt/n or $\frac{\lambda_0}{2n\gamma^2}\left(1+\frac{K^2}{2}\right)$ will stay in phase and interfere constructively
- Harmonics of the fundamental wavelength

Undulator

- Antenna emitting light of wavelength λ_0
- Doppler effect :

$$\lambda = (1-\beta)\lambda_0 = \frac{1-\beta^2}{1+\beta}\lambda_0 = \frac{\lambda_0}{2\gamma^2}$$

- X-rays !

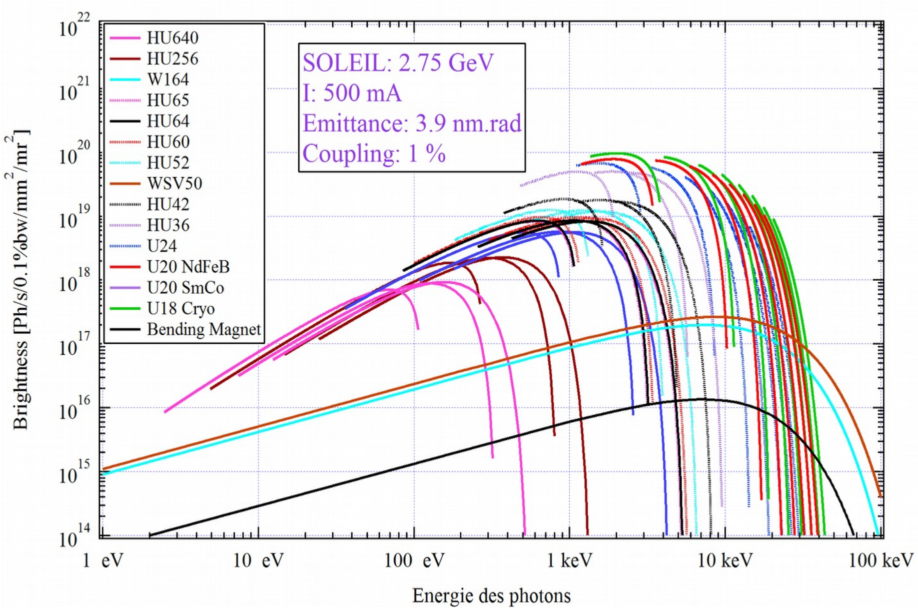

Synchrotron Radiation in astronomy

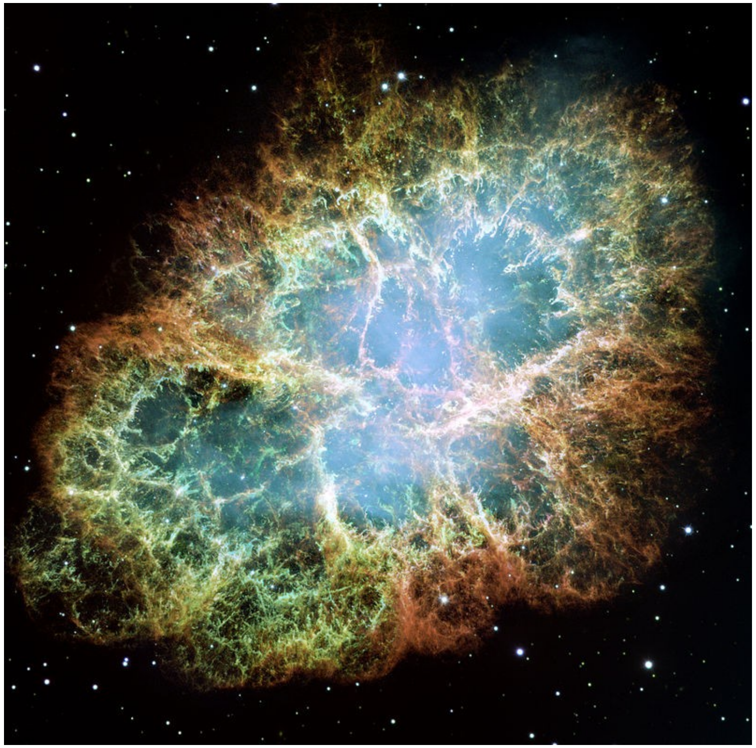

"Crab Nebula" by NASA, ESA, J. Hester and A. Loll (Arizona State University) -Hubble

- High magnetic fields
- Polarized light

First Synchrotrons

Goward F. K. and Barnes D. E., Nature, 158 413 (1946)
General Electric, 1946
Gooden J.S., Jensen H.H and Symonds J.L., ``Theory of the proton synchrotron'' Proc. Phys. Soc. 59, 677 (1947)
3GeV ``Cosmotron'', Brookhaven, 1952
Proton Synchrotron, Birmingham, 1953
...ACO, 1965
http://sciences-aco.lal.in2p3.fr/

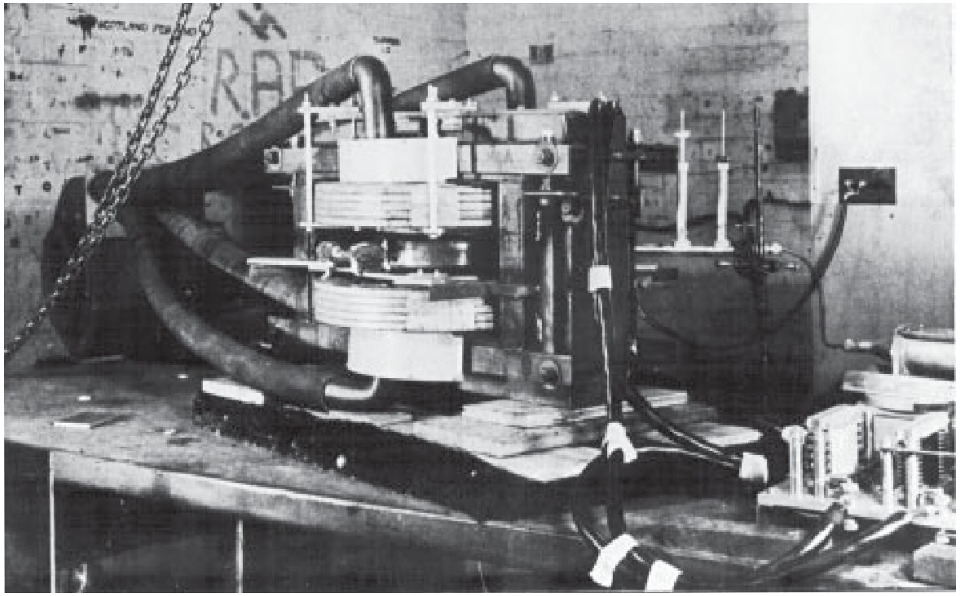

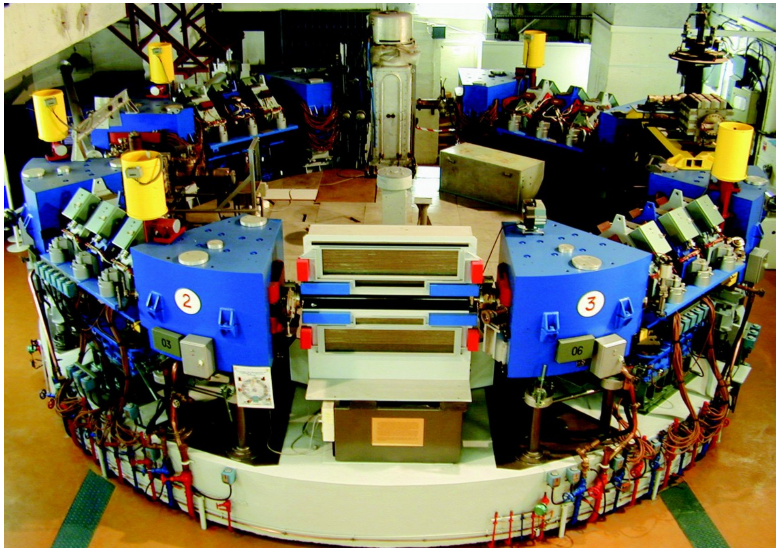

First Observation in a Synchrotron

General Electric 70MeV synchrotron, 1947
Elder F.R., Gurewitsch A.M., Langmuir R.V., Pollock H.C. ``Radiation from Electrons in a Synchrotron'' Physical Review 71, 829 (1947)
Blewett J.P. Physical Review 69, 87 (1946).

Electron Beam Optics

SOLEIL Lattice

ε_{x0} = 3.7 nm•rad @ 2.75 GeV

Circumference: **354 m**

24 straight sections

(variable length)

4 x 12 m
12 x 7 m
8 x 3.6 m

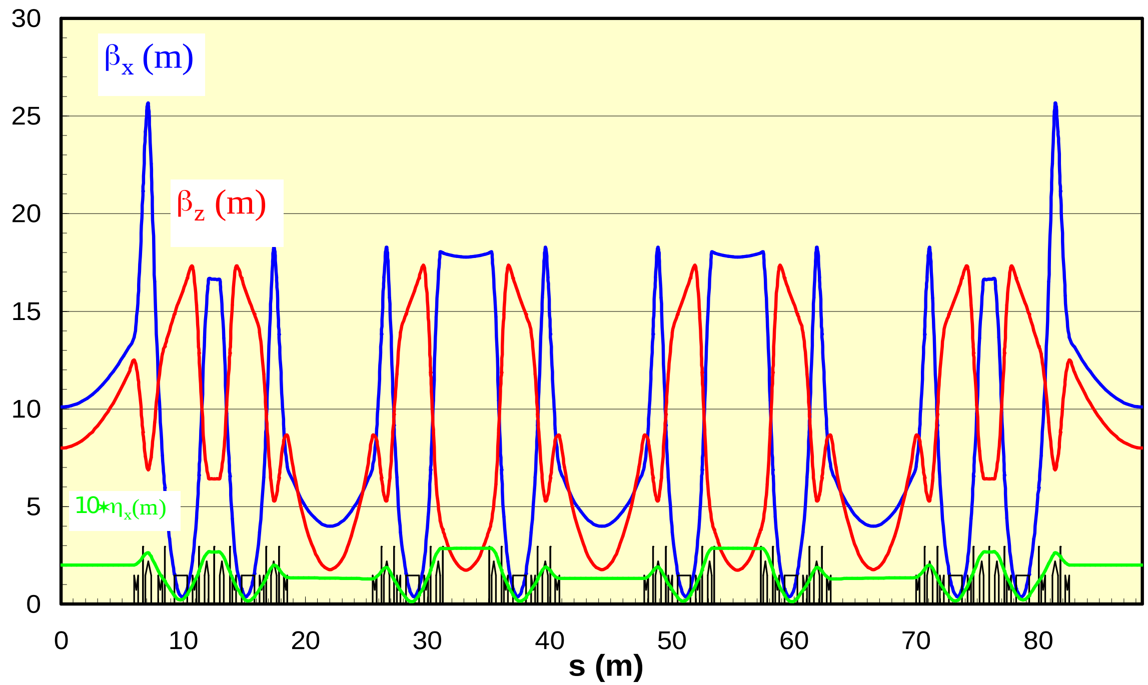

Accelerating Cavities

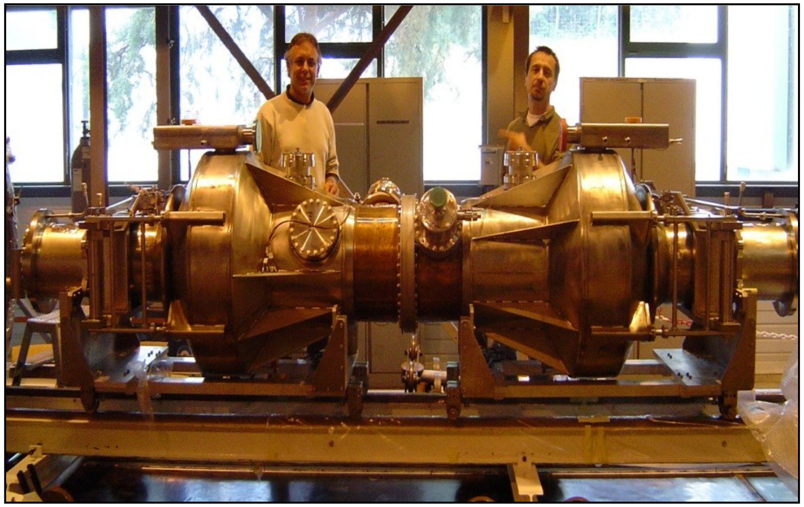

Amplifiers

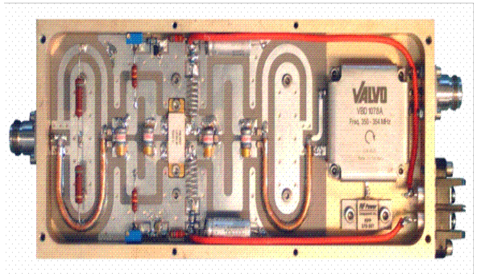

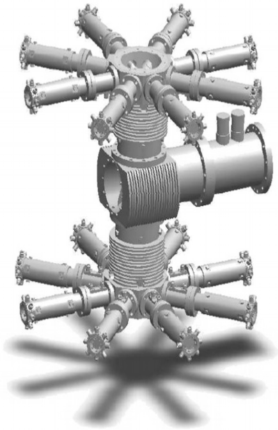

Insertion Devices

HU640

HU80

U20

HU256

Insertion Devices

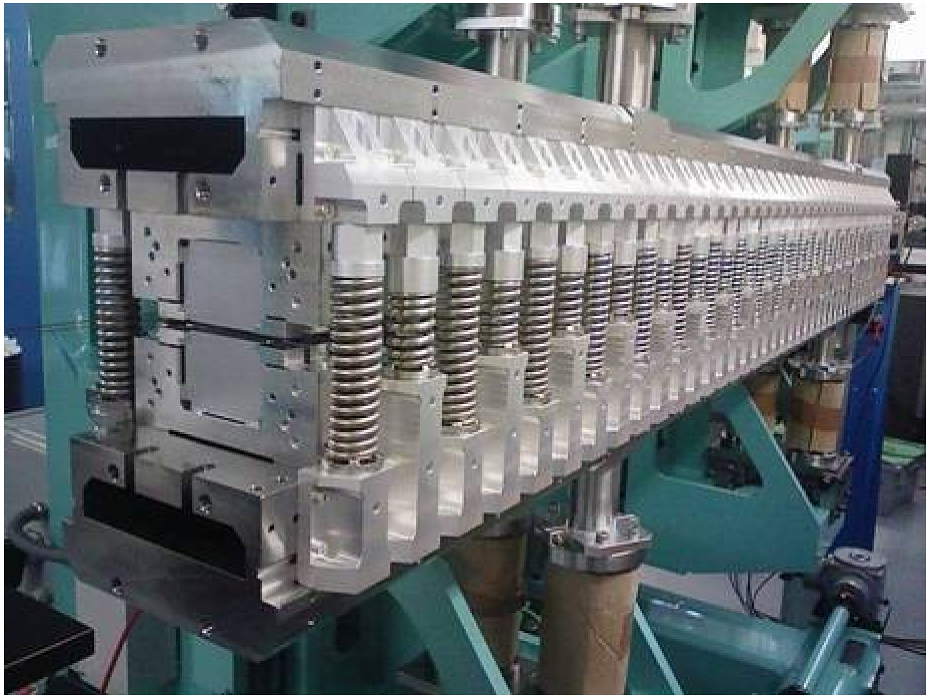

In-vaccum Wiggler (WSV50)

Electromagnetic/Permanent Magnets Planar Helical Undulator

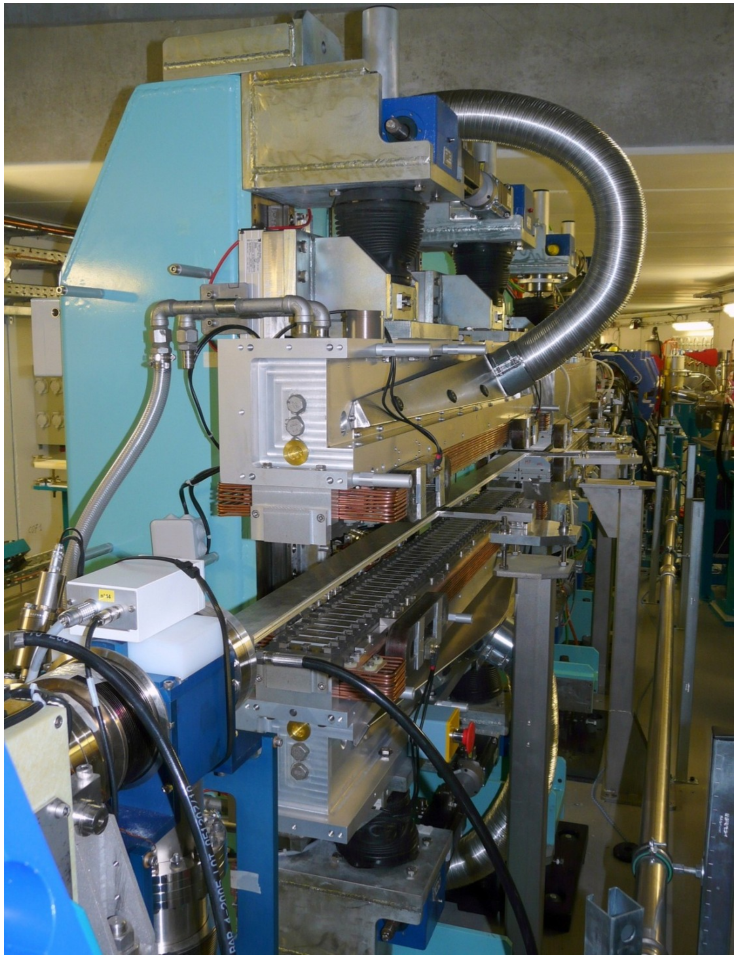

EMPHU

- Energy : monochromaticity, tunability or “white beam”, from THz to hard X-rays
- Beam size : from 10 nm to cms
- Brightness : up to 10^{21} photons/sec/mm²/mrad²/0.1\% BW)
- Time structure : picoseconds
- Polarization: linear and circular

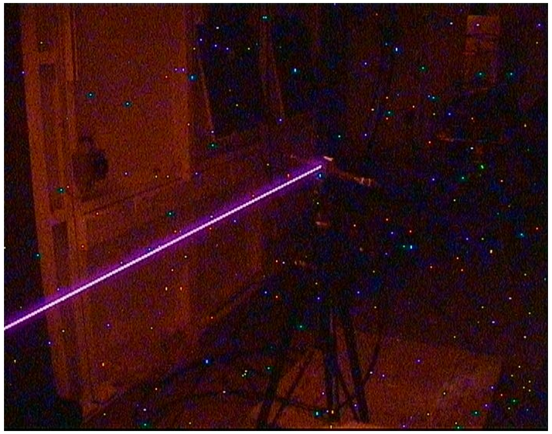

Stability

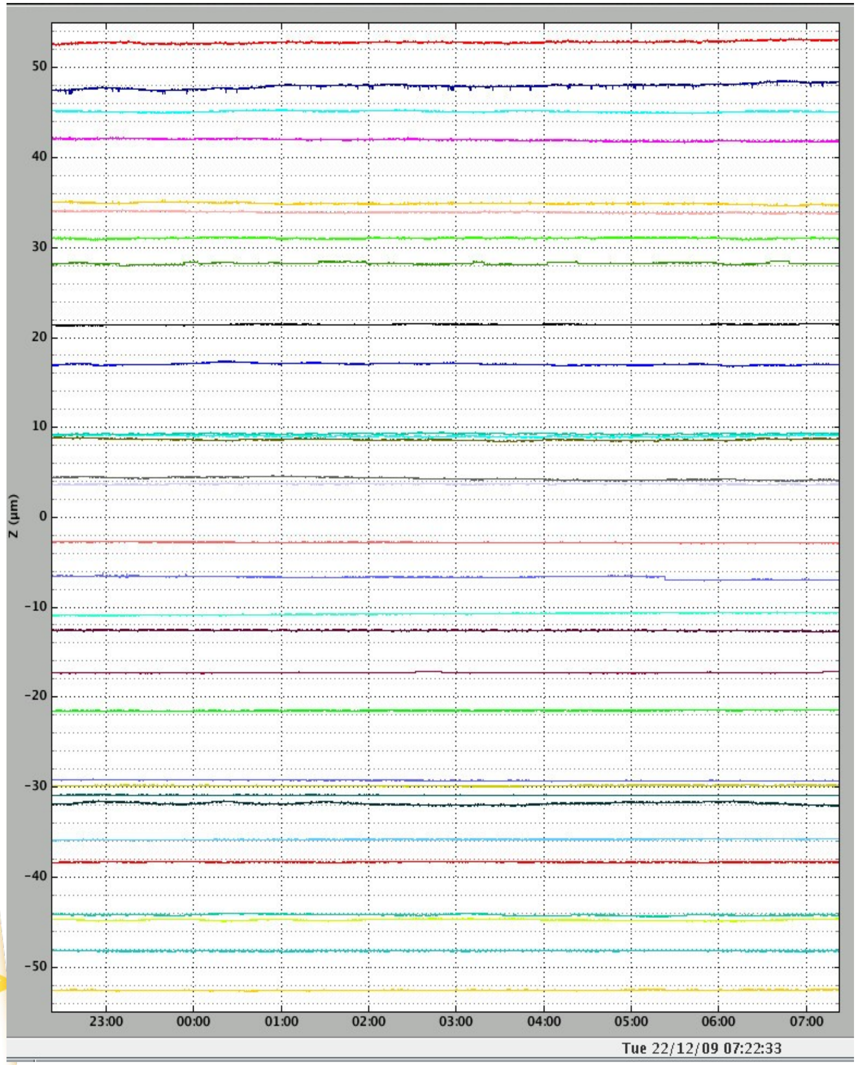
Z (µm)
50
40
30
20
10
0
-10
-20
-30
-40
-50
23:00
00:00
01:00
02:00
03:00
04:00
05:00
06:00
07:00
Tue 22/12/09 07:22:33

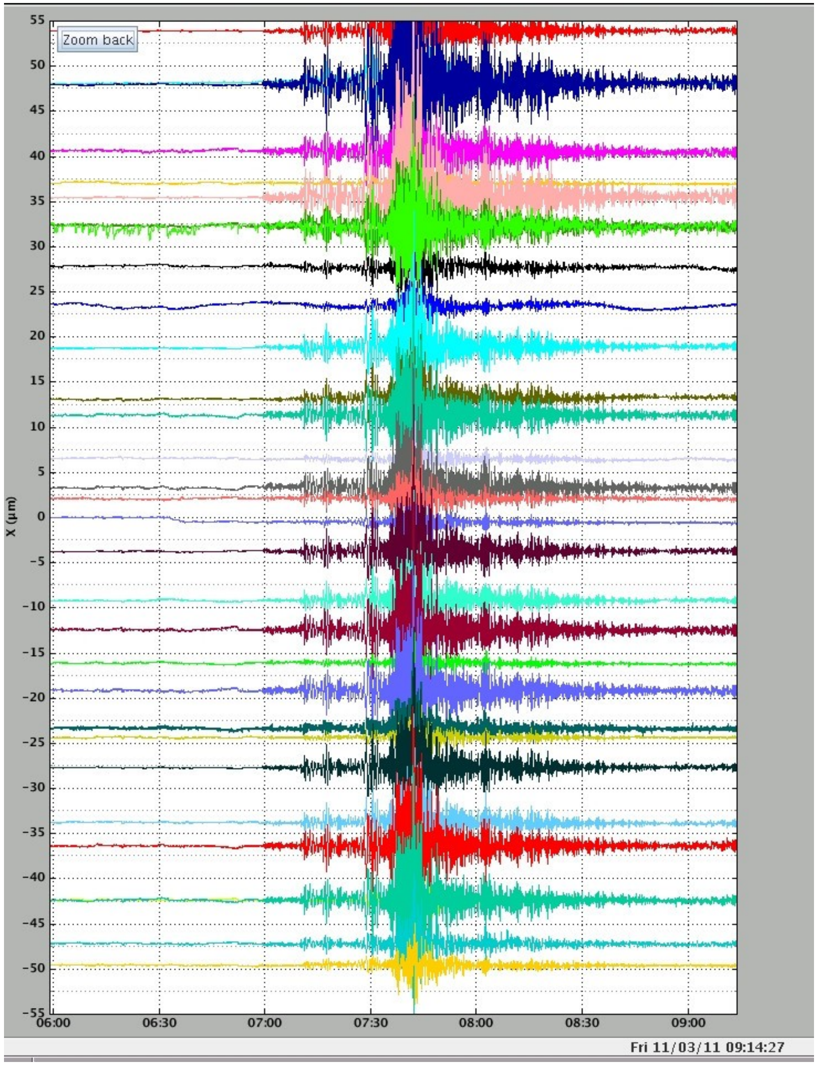
Zoom back
X (µm)
55
50
45
40
35
30
25
20
15
10
5
0
-5
-10
-15
-20
-25
-30
-35
-40
-45
-50
-55
06:00
06:30
07:00
07:30
08:00
08:30
09:00
Fri 11/03/11 09:14:27

Synchrotrons in the World

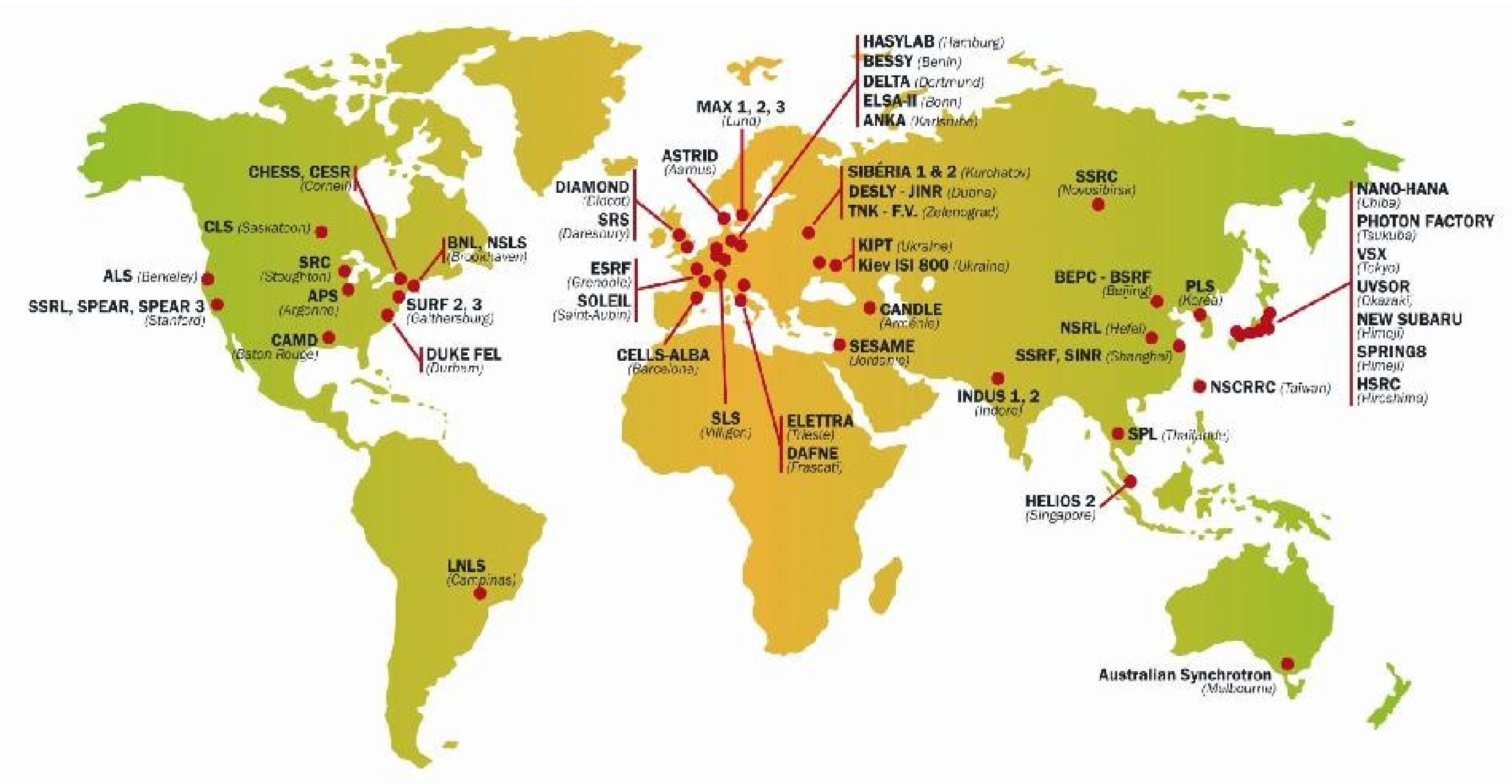

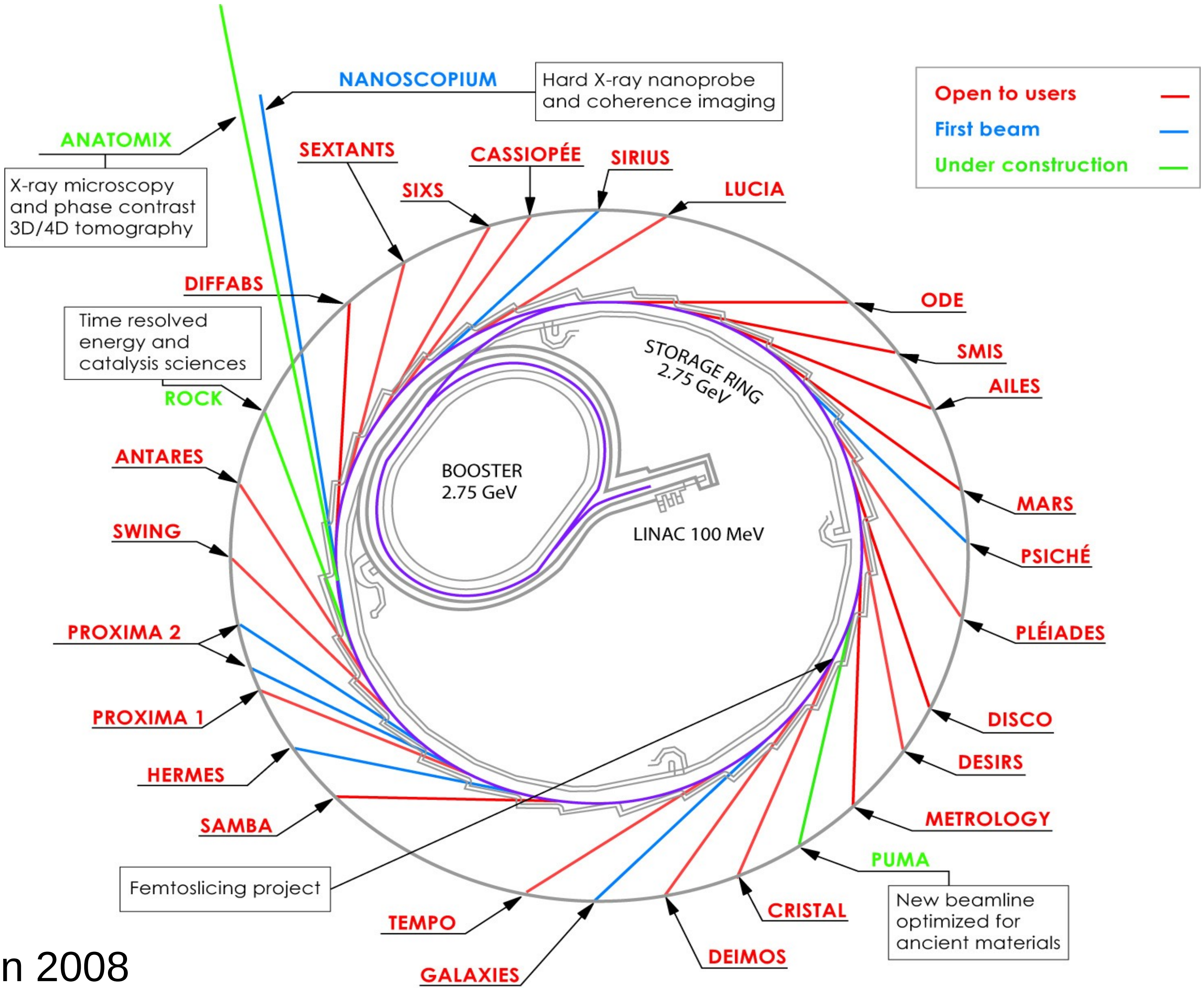

NANOSCOPIUM
Hard X-ray nanoprobe and coherence imaging
ANATOMIX
X-ray microscopy and phase contrast 3D/4D tomography
SEXTANTS
CASSIOPÉE
SIRIUS
LUCIA
SIXS
DIFFABS
Time resolved energy and catalysis sciences
ROCK
ANTARES
SWING
PROXIMA 2
PROXIMA 1
HERMES
SAMBA
Femtoslicing project
TEMPO
GALAXIES
DEIMOS
CRISTAL
PUMA
New beamline optimized for ancient materials
METROLOGY
DESIRS
DISCO
PLÉIADES
PSICHÉ
MARS
AILES
SMIS
ODE
Open to users
First beam
Under construction
STORAGE RING 2.75 GeV
BOOSTER 2.75 GeV
LINAC 100 MeV

Open in 2008

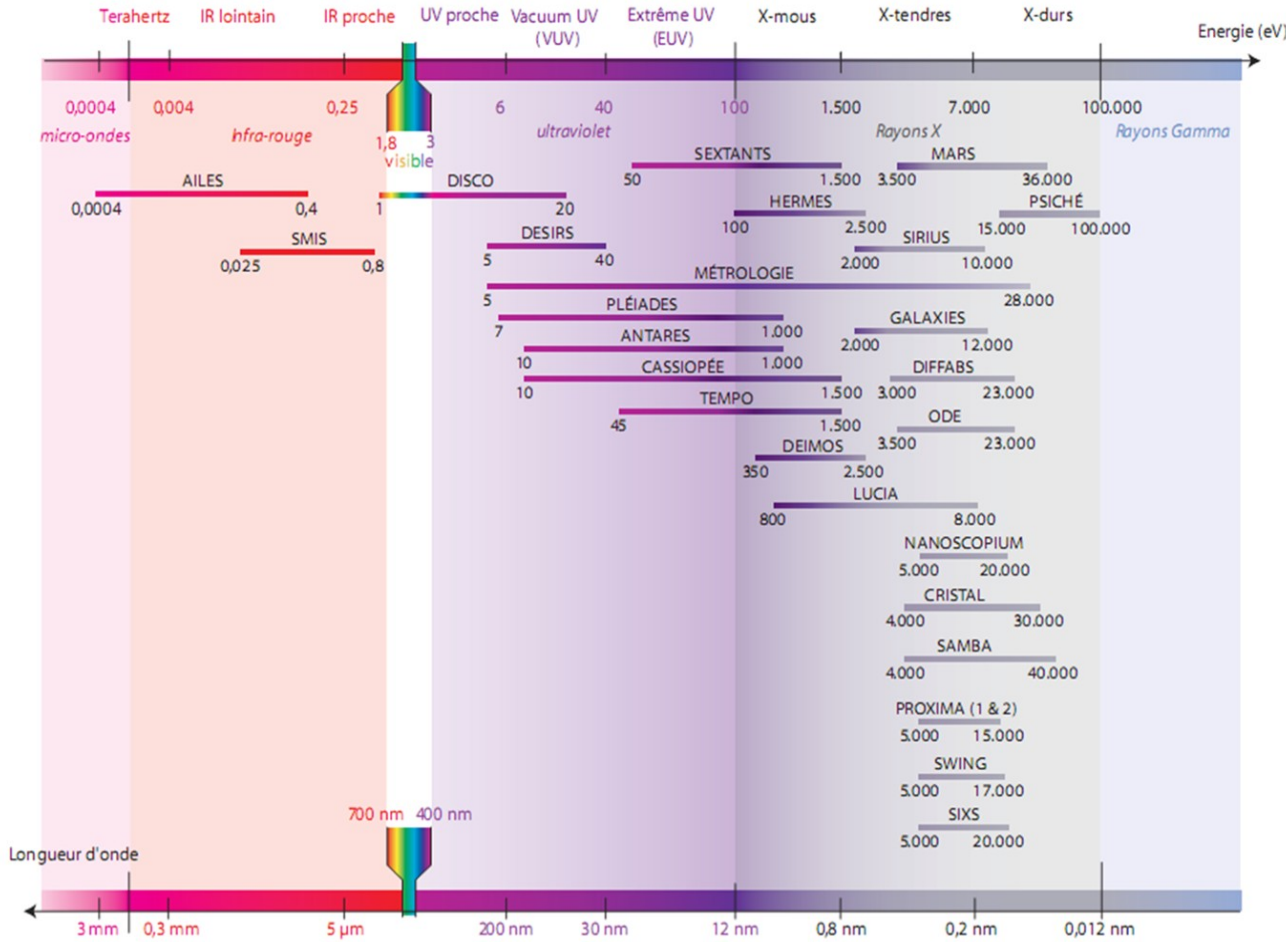

- 9 orders of magnitude in wavelength !
- Structure, electronic and magnetic properties, vibrations...
- Complementary experiments to study processes

Applications

Applications

- Elastic (Thomson) scattering
- Absorption / Fluorescence
- Photoelectric effect
- Anomalous scattering / Resonant scattering
- Inelastic scattering / Raman scattering / Compton
- Magnetic scattering

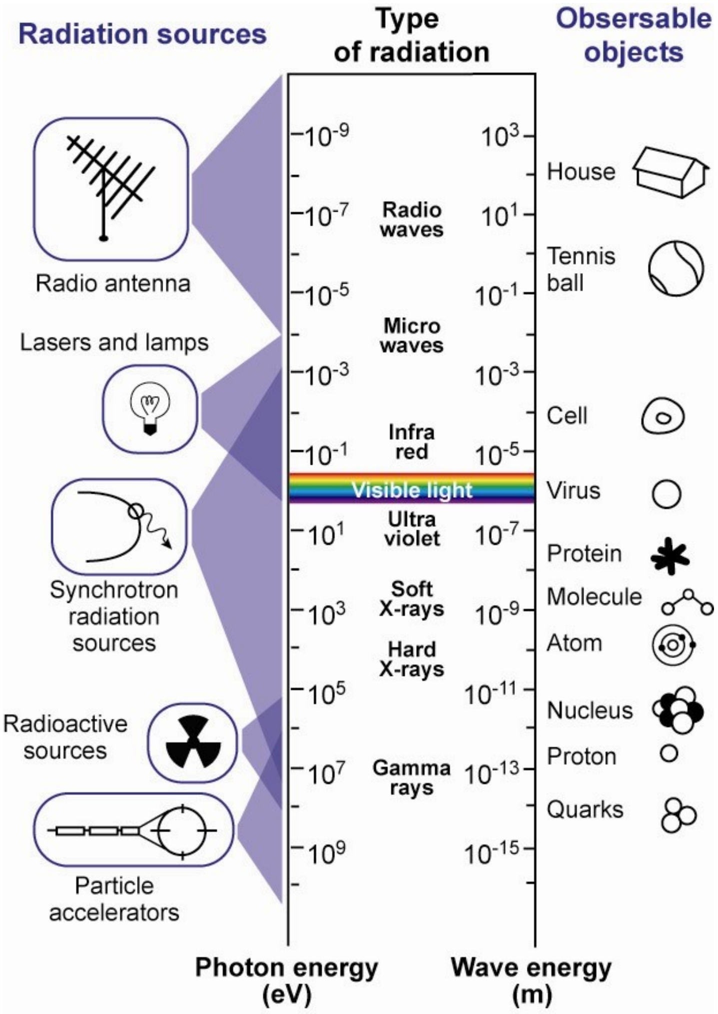

X-ray Optics

Kirkpatrik-Baez mirrors

P. Kirkpatrick and V. Baez, J. Opt. Soc. Am. 38, 766 (1948)

Achromatic
7nm achieved @ 20keV
H. Mimura et al. Nature Physics 6, 122 (2010)

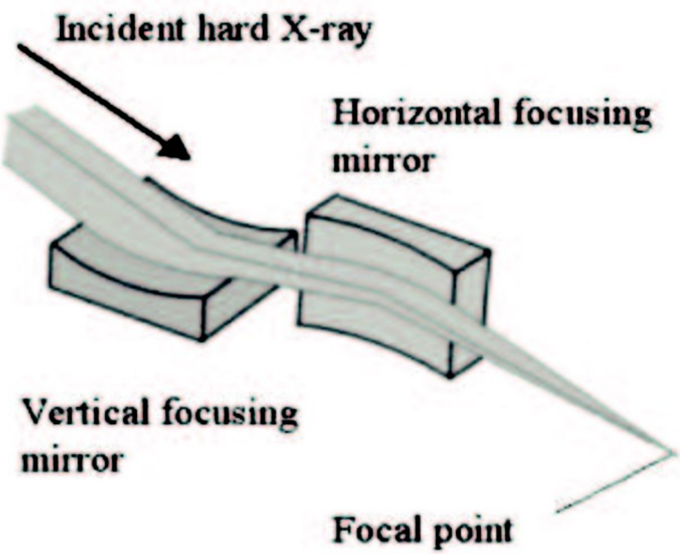

Compound refractive lenses

A. Snigirev et al. Nature 384, 49 (1996)

Low Z materials
Parabolic shape
Small N.A.10^{-4} to 10^{-3}
< 50nm, 10^8 ph/s

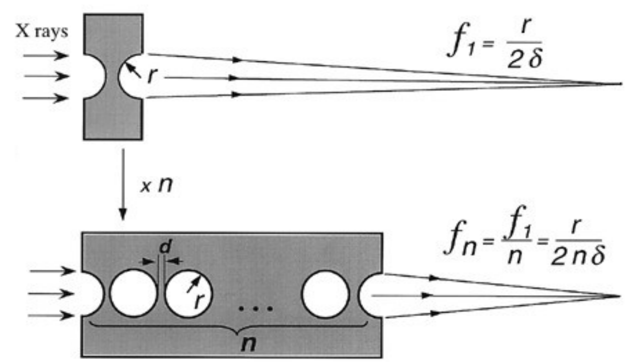

Fresnel construction

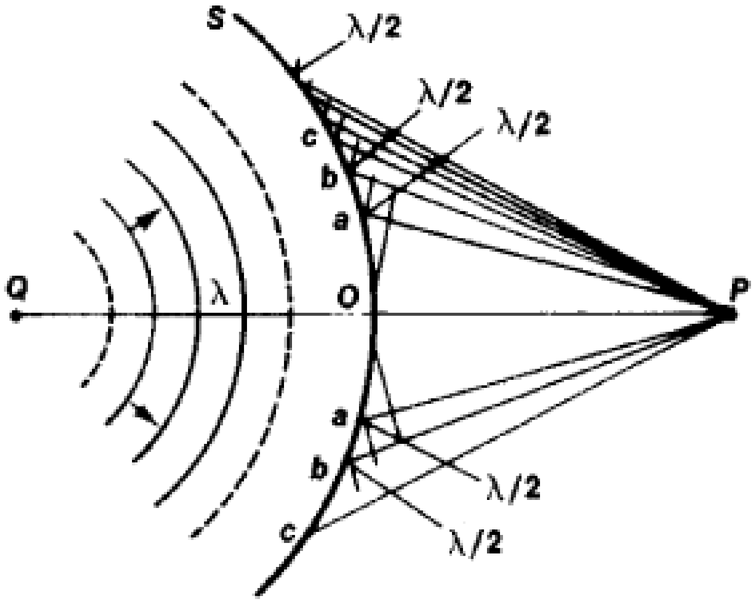

Neighboring zones
interfere destructively

Fresnel lens

Zone Plates

PSI-SOLEIL collaboration

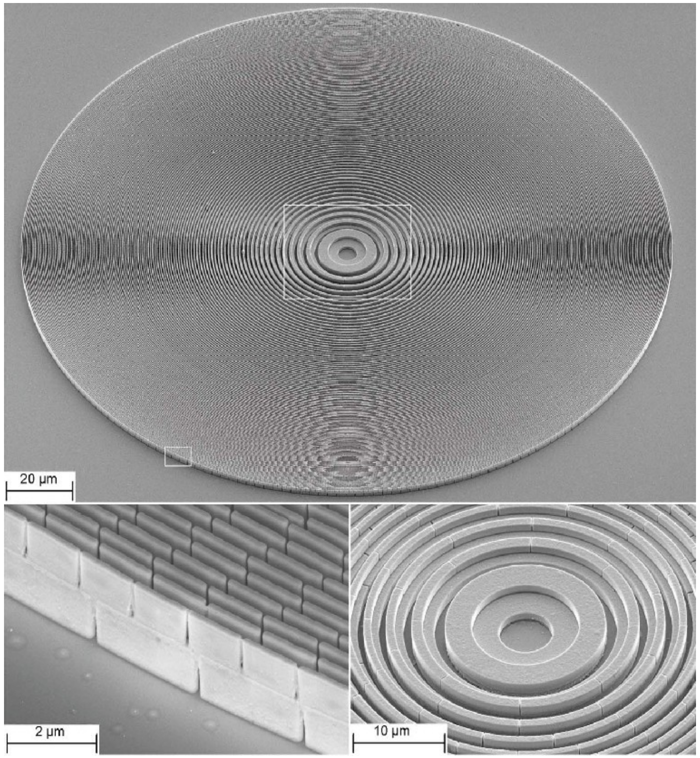

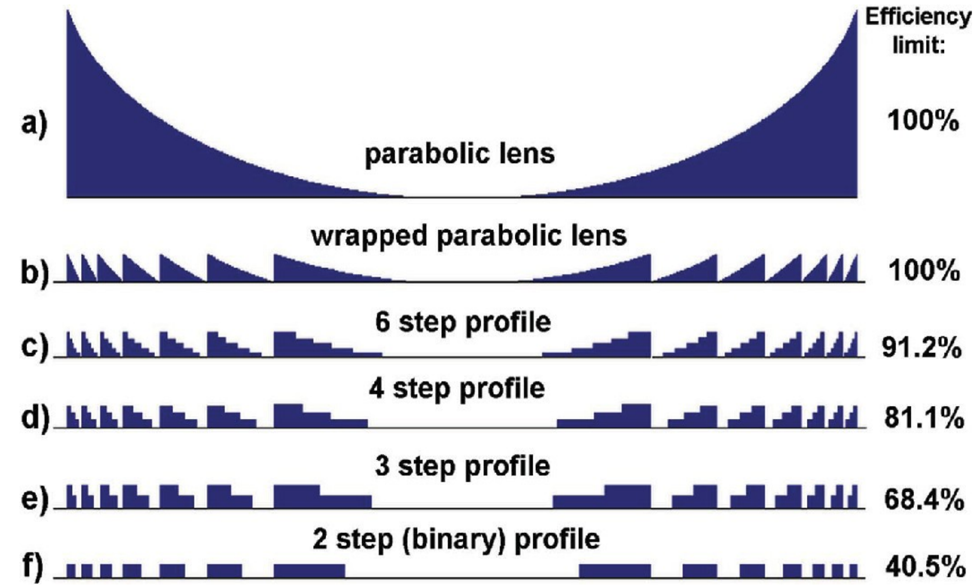

Mohacsi et al., J. Sync. Rad. 2014, Optics Express 2015

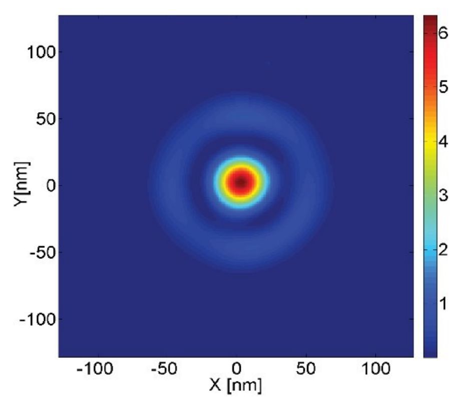

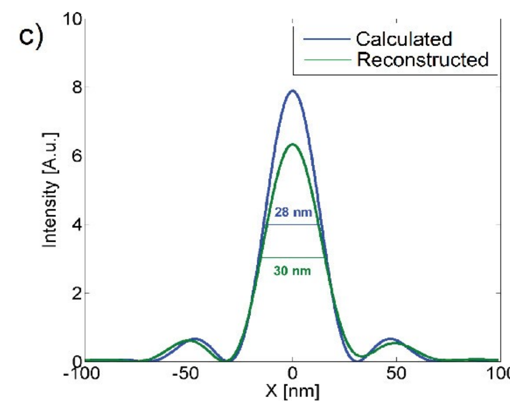

Efficiency 80 % @ 200nm
Efficiency 10 % @ 30nm

Macromolecular Crystallography

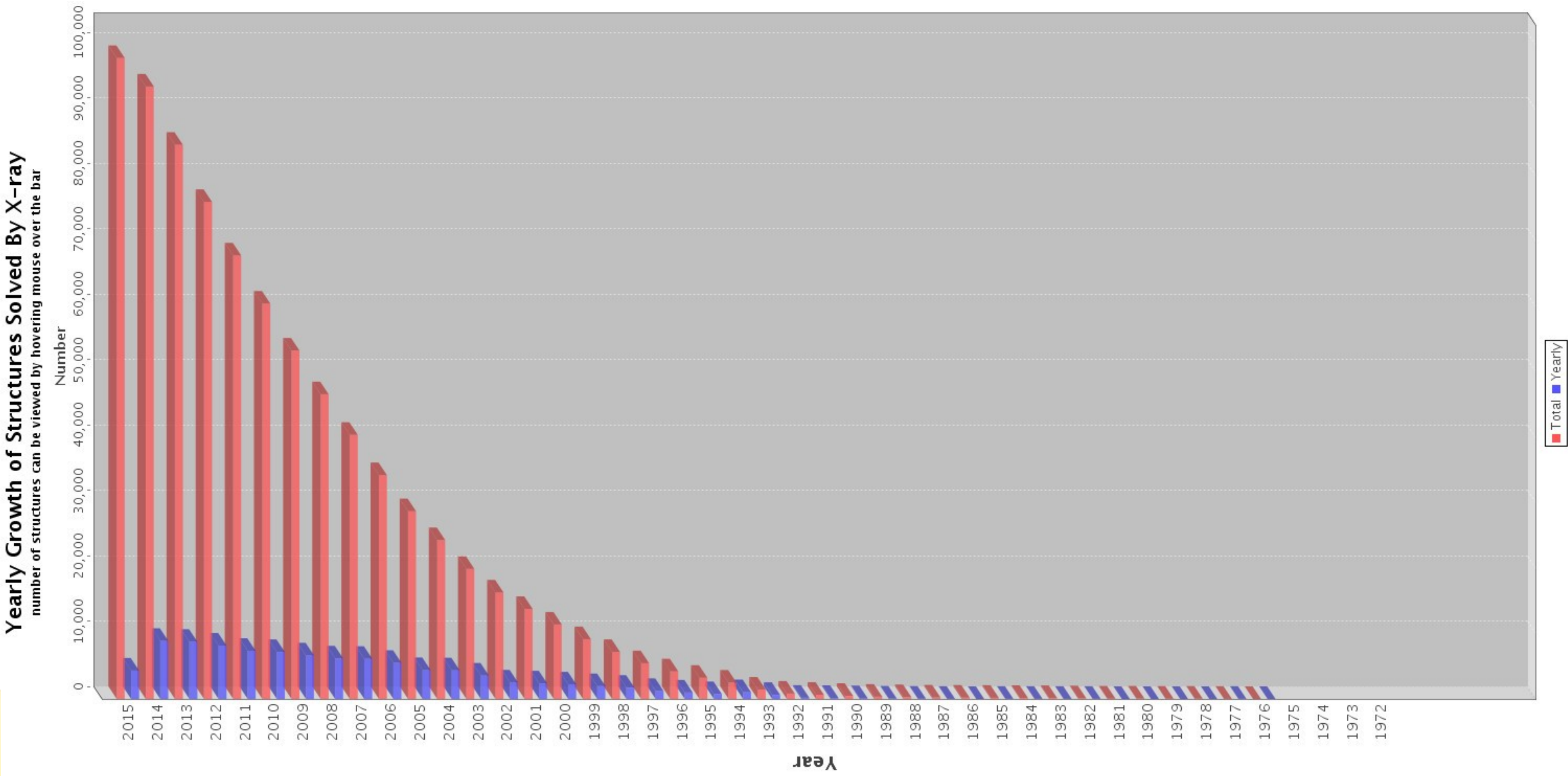

Protein Data Bank (PDB)

Also NMR (11000), electron microscopy (800)

Macromolecular Crystallography

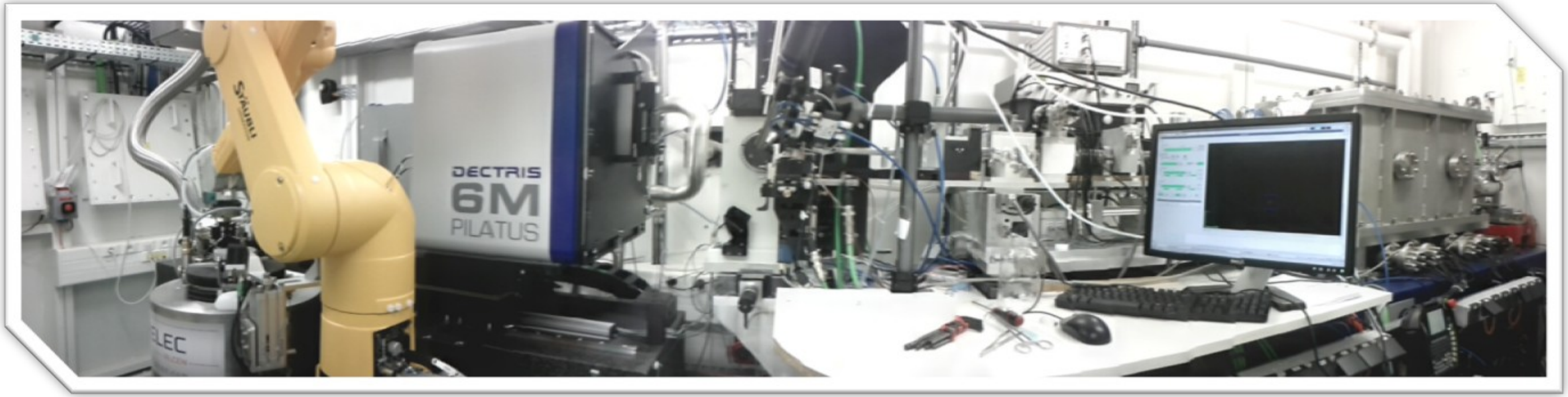

Energy range 6 keV – 15.5 keV.
Beam size at sample variable from 50 x 50 microns to 200 x 100 microns.
CATS robot (48 samples) or plate screening.
PILATUS 6M detector (25 Hz)
Crystal Logic 3 circle goniometer

Macromolecular Crystallography

Structural basis for the inhibition of the eukaryotic ribosome

Nature 2014

Nicolas Garreau de Loubresse[1], Irina Prokhorova[1], Wolf Holtkamp[2], Marina V. Rodnina[2], Gulnara Yusupova[1] & Marat Yusupov[1]

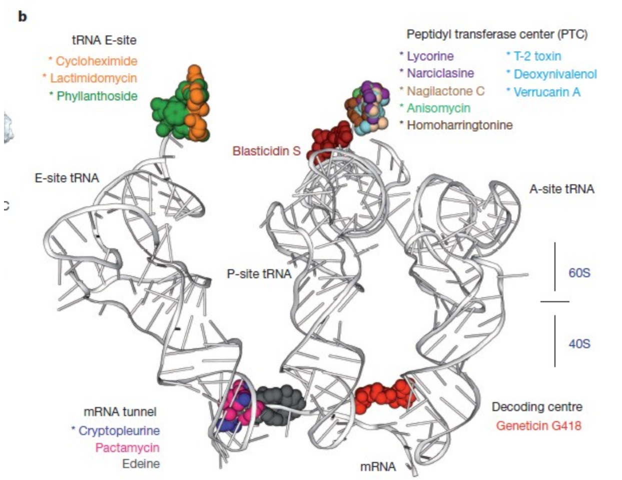

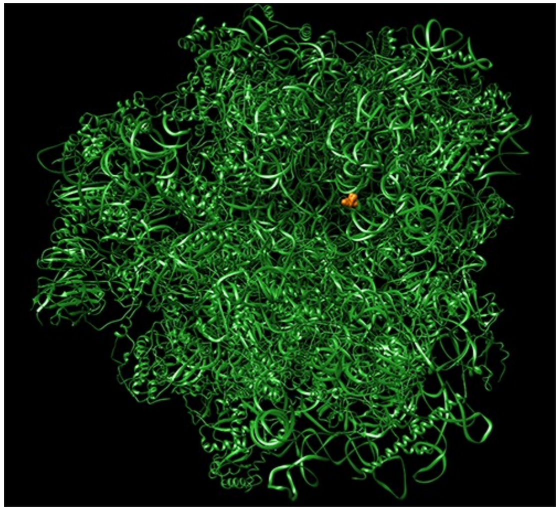

- 3.3 MDa yeast ribosome, significantly bigger than bacterial ribosomes.
- Optimisation of crystal treatment (cryo-protection, preparation in cold room). $P2_1$ 303 x 286 x 435 Ǻ, β=99°.
- Soaking of different naturally occuring inhibitors, some broad spectrum, some eukaryotic specific.
- Structure of 16 ribosome inhibitor complexes determined on PROXIMA 1.
- When compared with inhibitor studies in bacterial ribosomes, sheds light on inhibitor specificity.

Data Collection

X-rays focussed « behind detector » to give almost parallel beam.
Size of beam limited by succession of slits and apertures, which reduce background, limit volume of crystal exposed and limit overall beam intensity.
Careful reduction of air scattering background. Data collection with photon counting pixel array detector.
« Gentle data collection », translating small beam across large crystal.

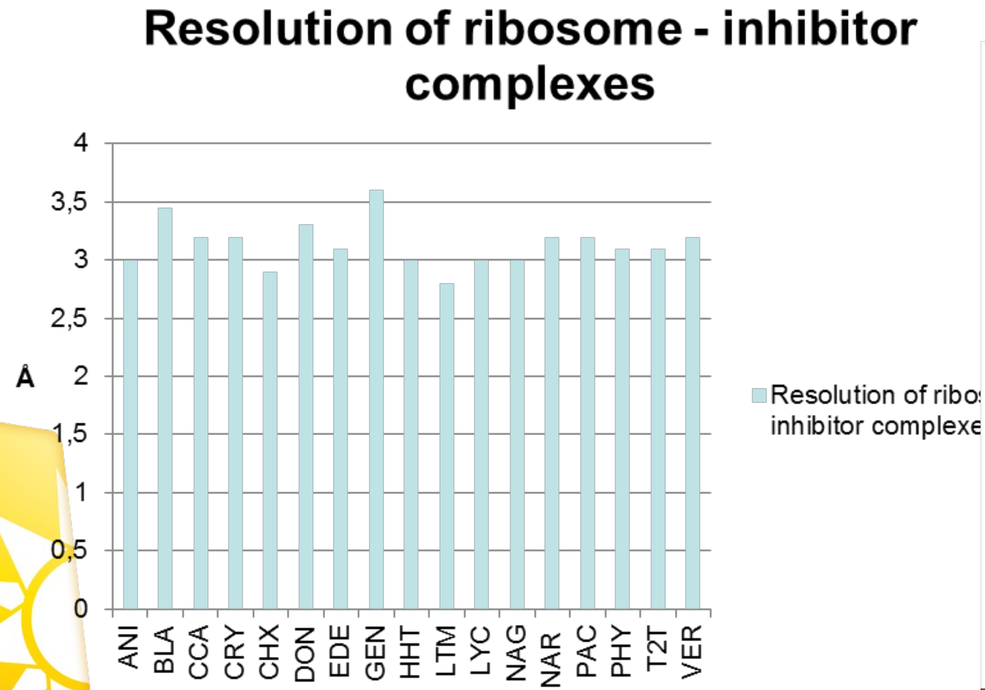

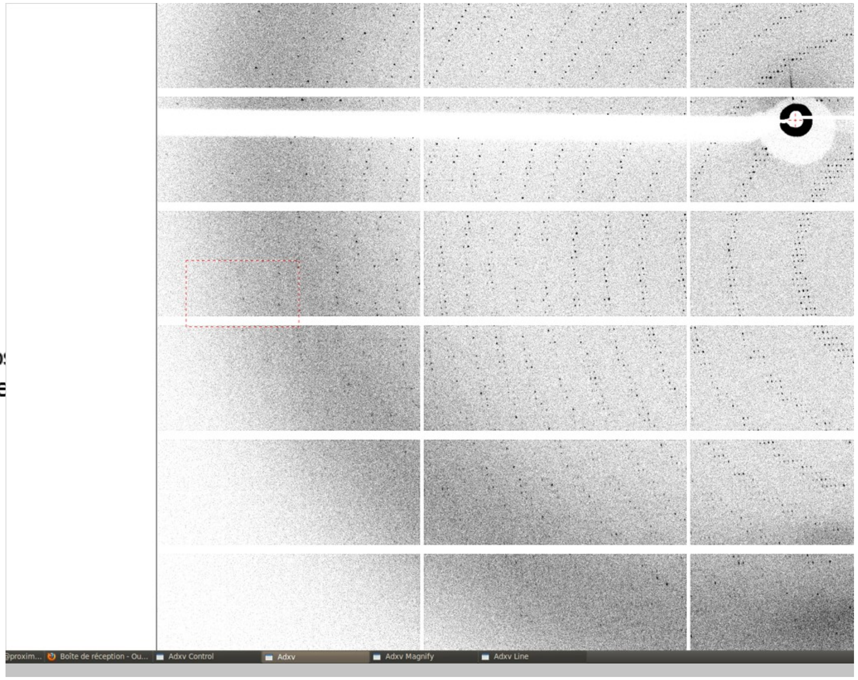

Screening for the best crystals

Small, aggregated, fragile crystals

- Automated Crystal Recognition
- Employing Artificial Intelligence
- Automated Grid & Helical Scans
- Finding the "sweet" spot of a crystal
- Merging Diffraction data
- From many zones of a larger crystal
  - Improve multiplicity for SAD phasing
- From many small crystals
  - Complete partial data sets
- In situ Data Collections
- From crystallisation plates
- From micro-fluidic chips

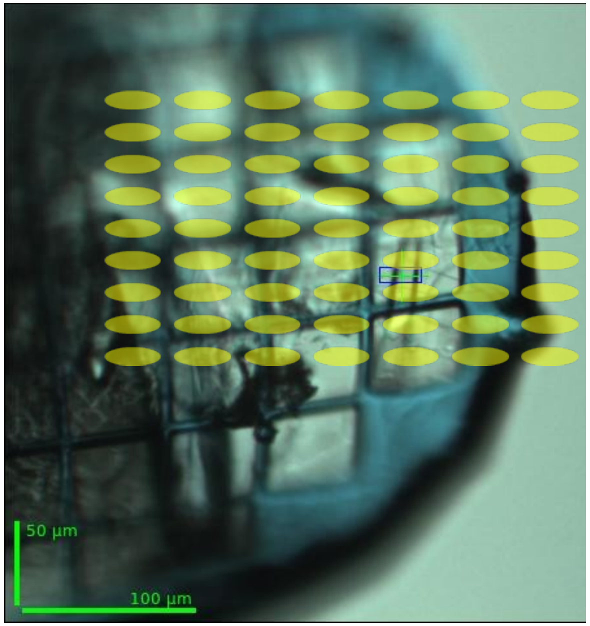

μ-fluidic chips

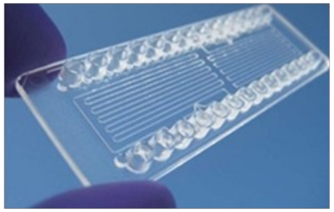

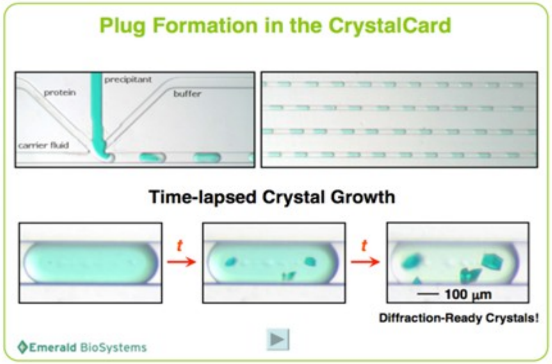

Small Angle X-ray Scattering

SOLEIL SYNCHROTRON

SWING

Modeling Detergent Organization around Aquaporin-0 Using Small-Angle X-ray Scattering

Alice Berthaud, John Manzi, Javier Pérez, and Stéphanie Mangenot (2012), J.A.C.S., 134, 10080-88.

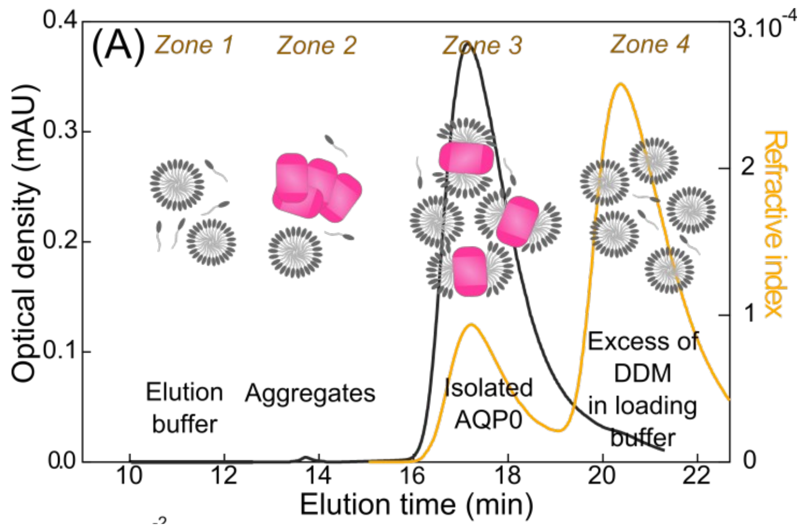

Solubilization of integral membrane proteins in aqueous solutions requires the presence of amphiphilic molecules like detergents. The presence of the detergent corona has strongly hampered structural studies of solubilized membrane proteins by SAXS. Through the online combination of size exclusion chromatography, SAXS, and refractometry, The authors have determined a precise geometrical model of the n -dodecyl β- D-maltopyranoside corona surrounding aquaporin-0, the most abundant membrane protein of the eye lens. The present protocol is a crucial step toward future conformational studies of membrane proteins in solution

Number of detergent molecules in the corona independently determined refractive index measurements /UV vis and SAXS I(0)/ UV vis, converging to very similar values.

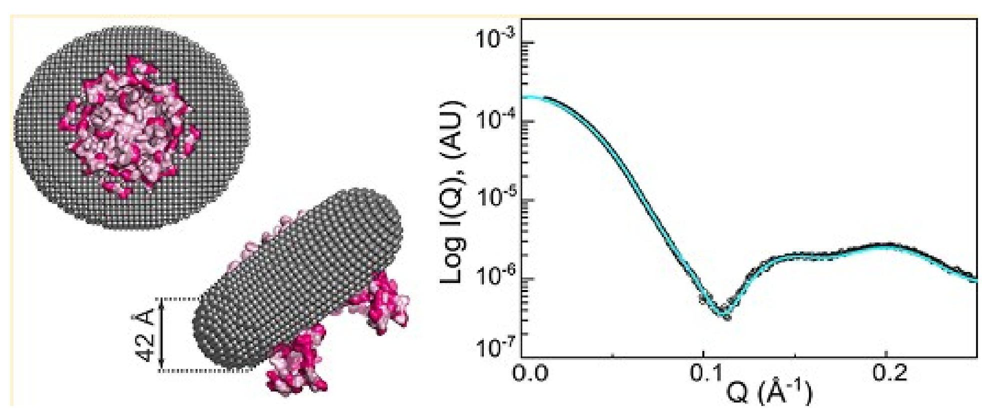

Small Angle X-ray Scattering

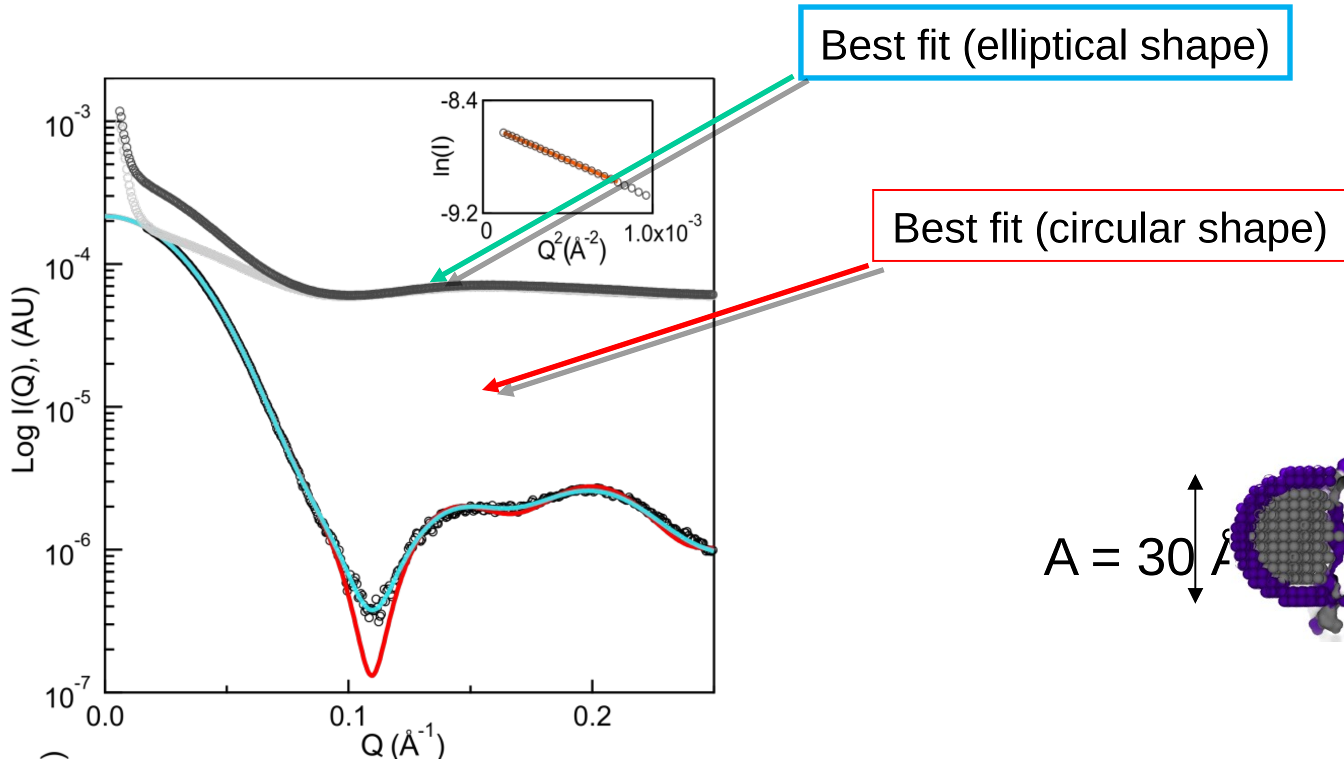

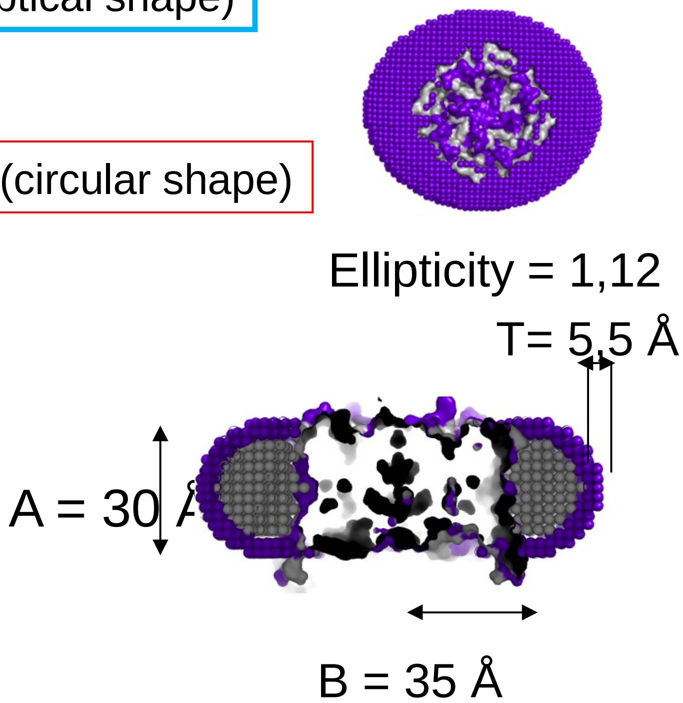

→ **Relevance of the model :**

- **Parameters physically meaningful**
- **N_{Det} = 270 ± 30 molecules per protein**

→ **Accuracy of the model :**

- **The fit is very sensitive to a small variation**

The belt model provides a structural basis to further study conformational changes → can be generalized to other membrane proteins

In-situ analysis of carbon nanotubes growth

Landois et al. Phys. Status Solidi **B 248**, 2449 (2011)

- Furnace specially designed for diffraction on 6-circles
- Use of XPAD detector for time resolved studies (1 image/s)
- Aerosol assisted catalytic chemical vapour deposition of carbon nanotube forest
- Toluene and ferrocene precursors injected @4Hz in He flow @ 850°C
- Possible to follow both nanotube and catalyst

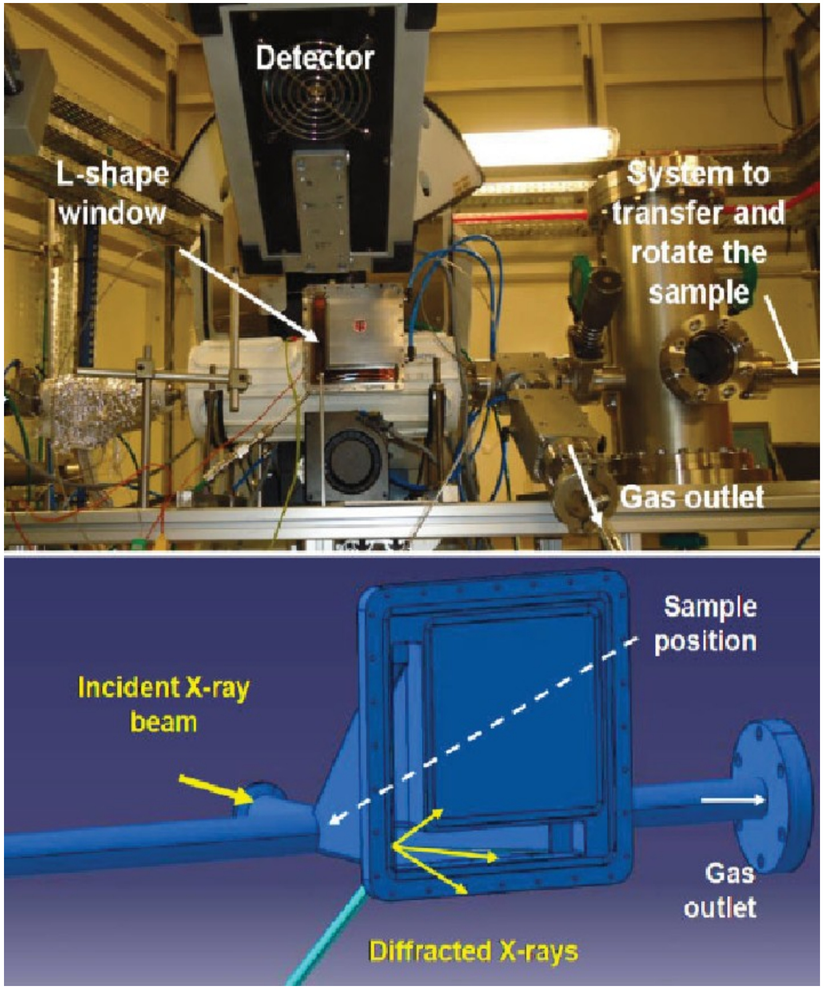

ANR : Lab. Francis Perrin, Lab. Physique des solides

In-situ analysis of carbon nanotubes growth

SEM of sample after 30s growth: Clean and well-aligned carbon nanotubes

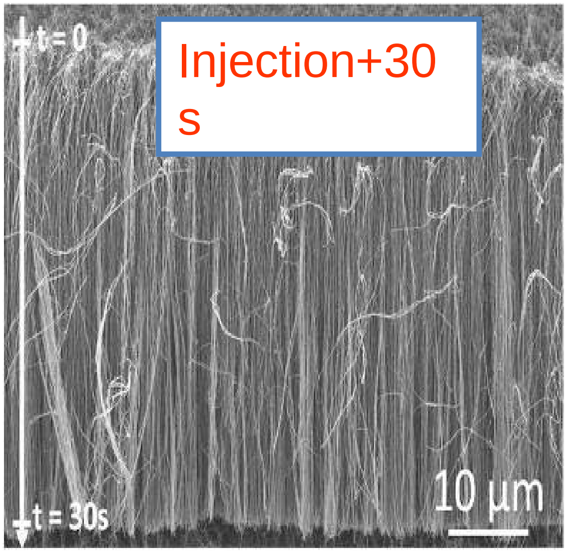

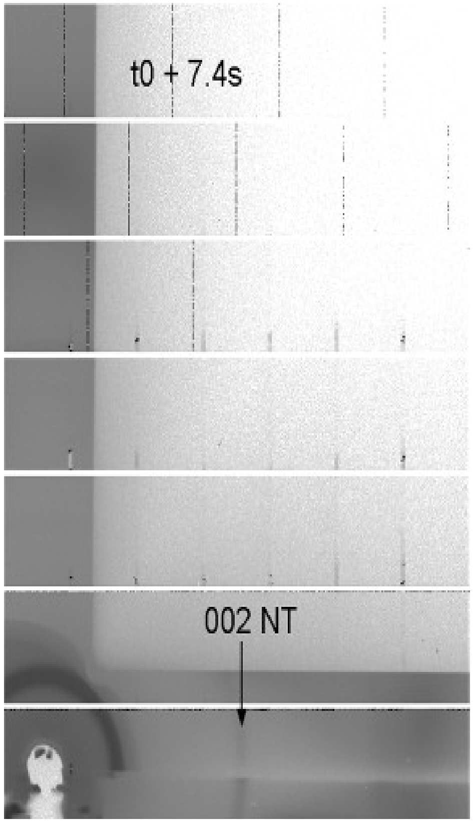

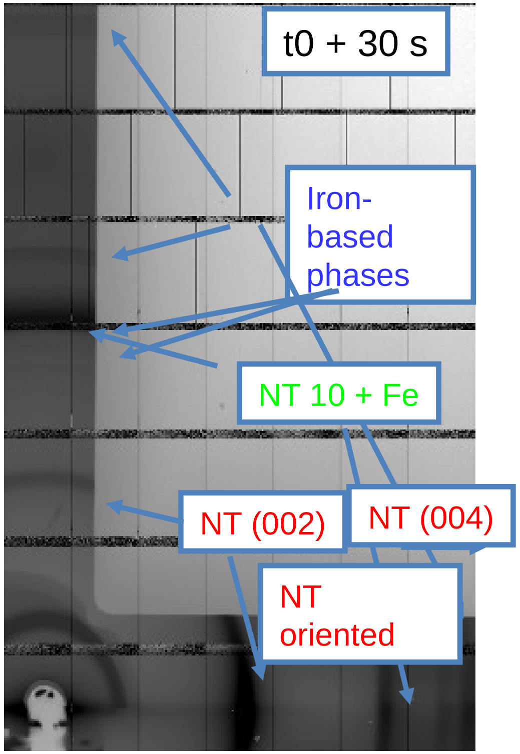

- Growth can be followed quantitatively
- Induction time ~ 25s before nanotube growth
- Fe_3C (cementite) appear first, 4s before CNT and may be the catalytic phase
- Order parameter increases from 0.3 to 0.8 after 60s

Infrared microscope

Small sample zone for materials <10 mm) and to attain pressures > 200 Gpa

Boehler-Almax high pressure cell

Horizontal microscope designed at SOLEIL

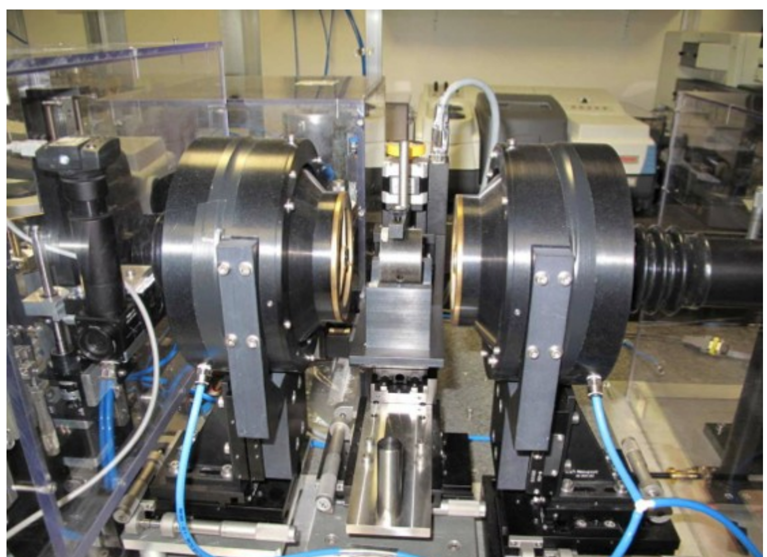

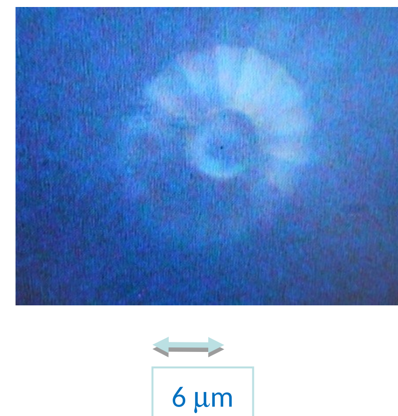

Metallic Hydrogen ?

Collaboration: Paul Loubeyre and Florent Occelli (CEA-DAM), Paul Dumas (SOLEIL)

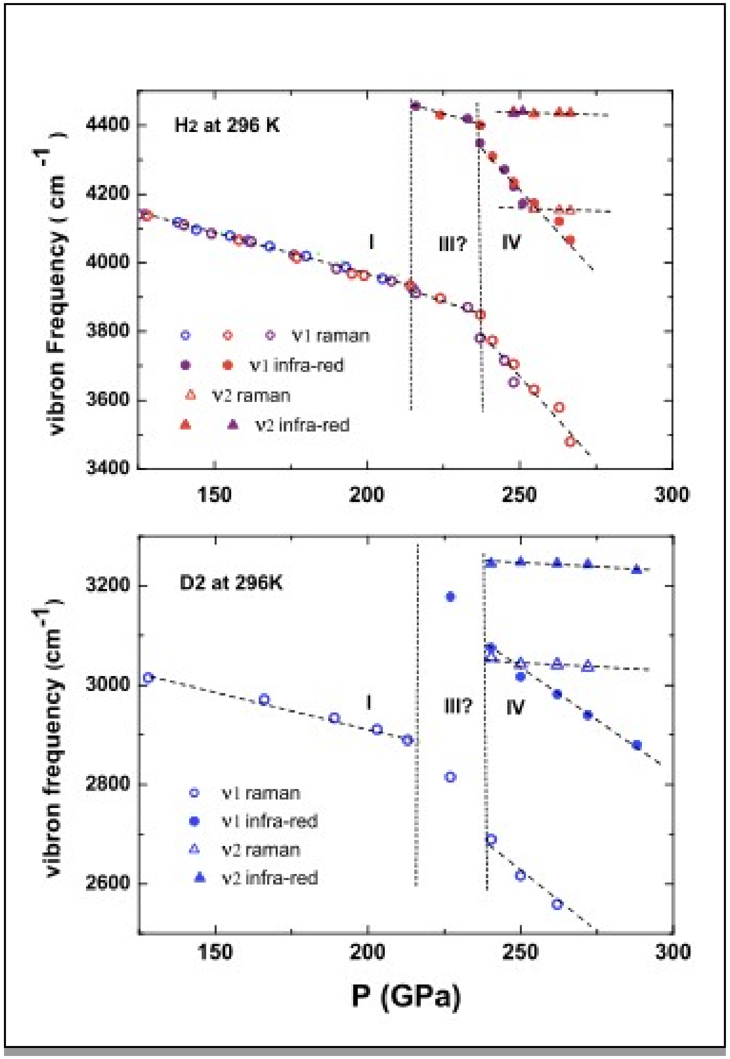

New non-metallic phase IV

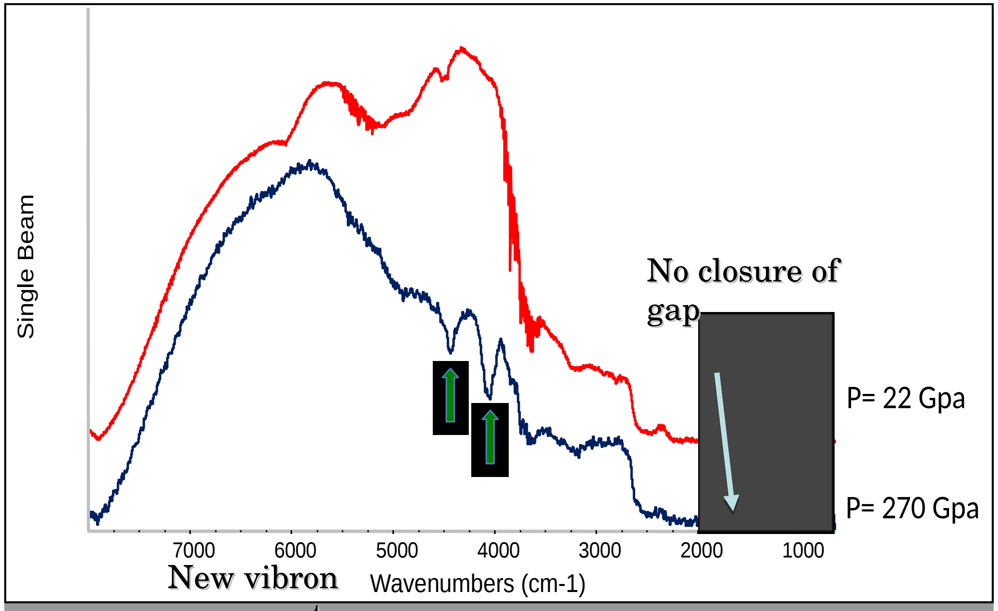

New vibron appears at 270GPa

Phys. Rev. B 87, 134101 (2013)

December 2014 new pressure record : 387 Gpa
But not yet the expected metallic transition of H2.

Another path to metallization : Lithium hydrides

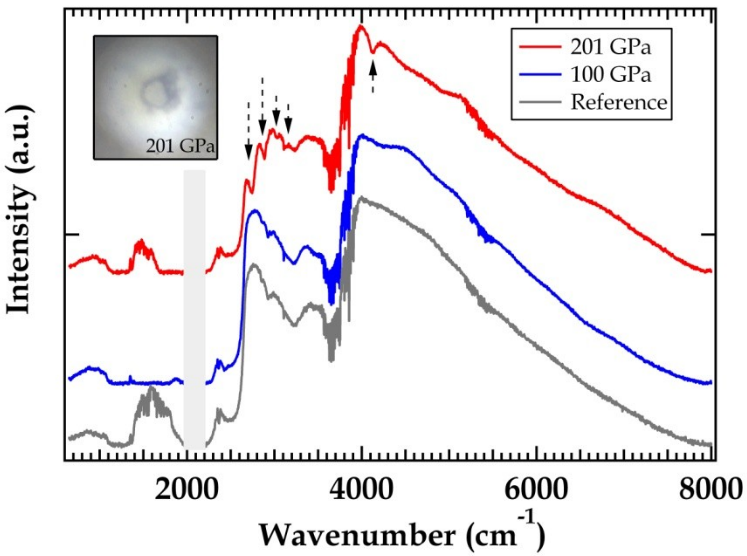

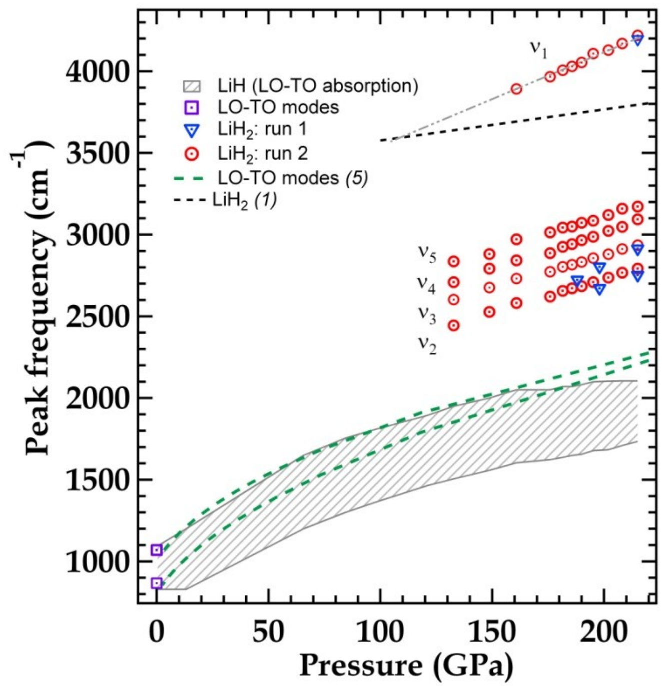

LiH2 modes

LiH modes

Evidence for LiH_2 and perhaps LiH_6 above 133 GPa, existence predicted in 2002.

Ch. Pepin, F. Occelli, P. Dumas and P. Loubeyre (PNAS, 2015)

A little bit of lithium does a lot for hydrogen

Eva Zurek[a,1], Roald Hoffmann[a,2], N. W. Ashcroft[b], Artem R. Oganov[c,d], and Andriy O. Lyakhov[c]

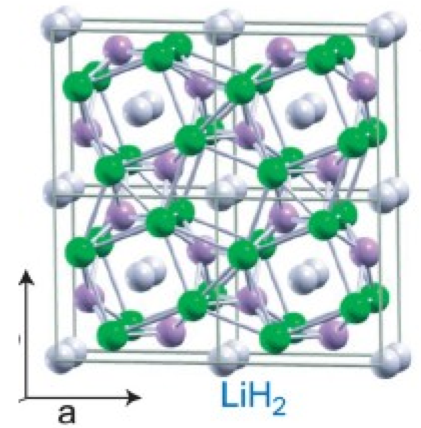

Bohr-Einstein Gedanken Experiment

In the 1920's Bohr and Einstein discussions led to a Gedanken experiment involving a double slit with a moving slit

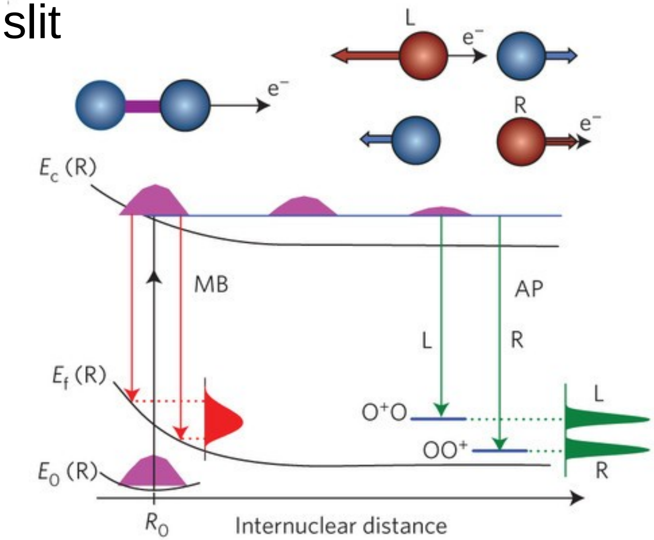

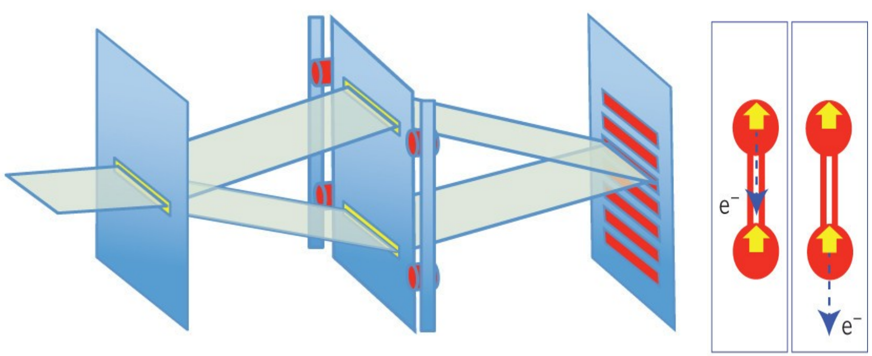

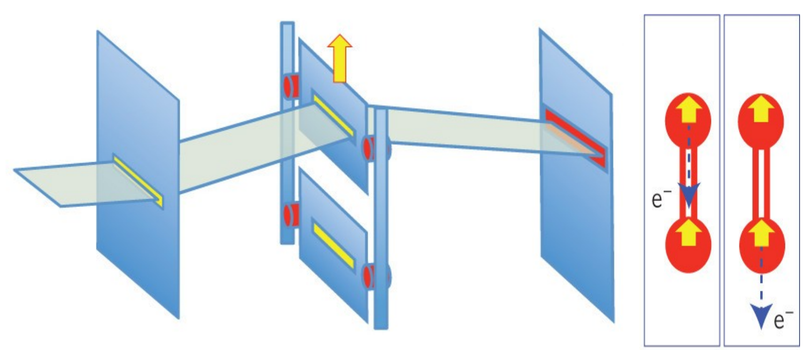

The 2 slits are coupled :
Impossible to determine from which slit the e^- has been ejected

The 2 slits are decoupled :
The asymmetric momentum transfer distinguishes the path (which slit the e^- has emerged from)

Bohr-Einstein Gedanken Experiment

Electron-ion coicidence allows the measurement of the momentum exchange between the Auger e⁻ and the atomic or molecular ion

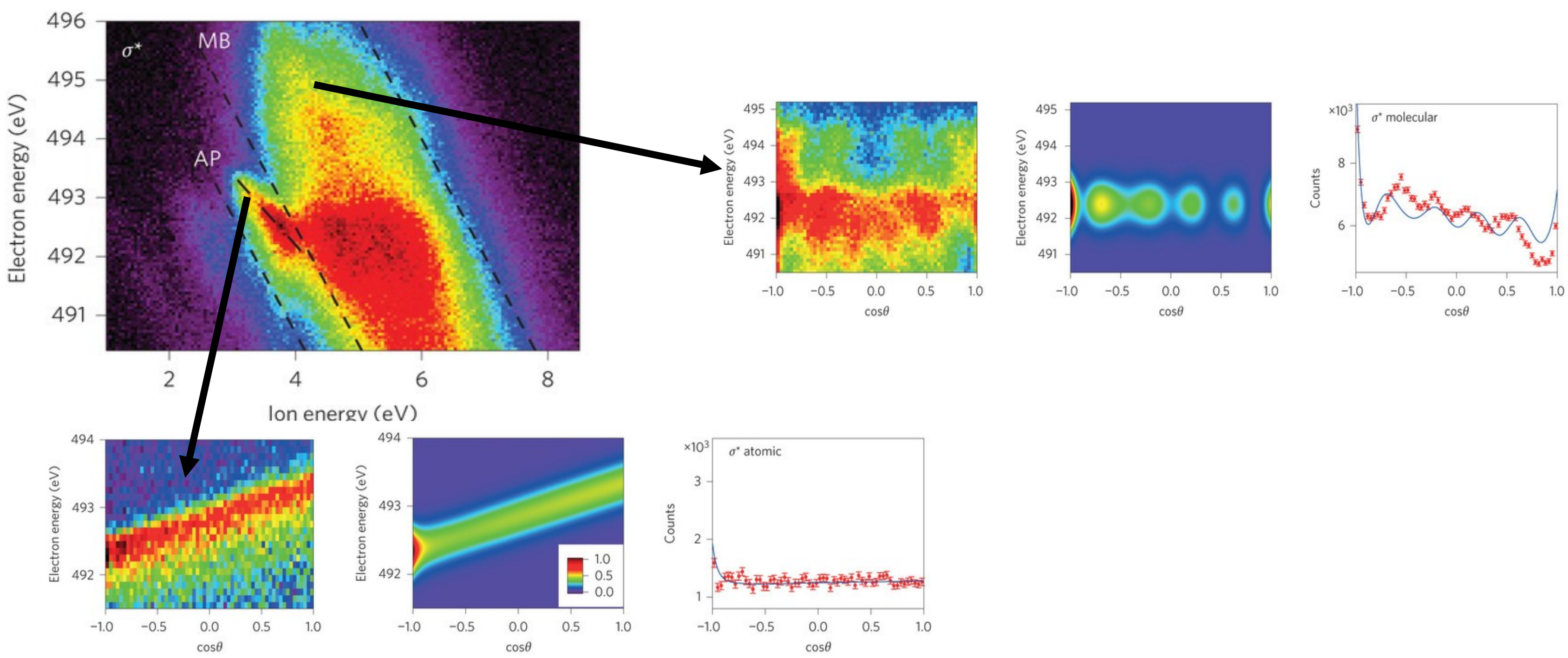

In complete agreement with Bohr's complementarity principle

Liu et al., Nature Photonics 2014

Synthesis of Gold Nanorods

$HAuCl_4$ + CTAB + $AgNO_3$ + Ascorbic Acid

Seeds formed in-situ $NaBH_4$

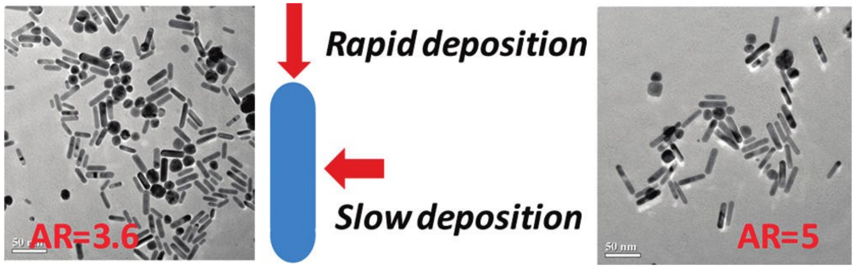

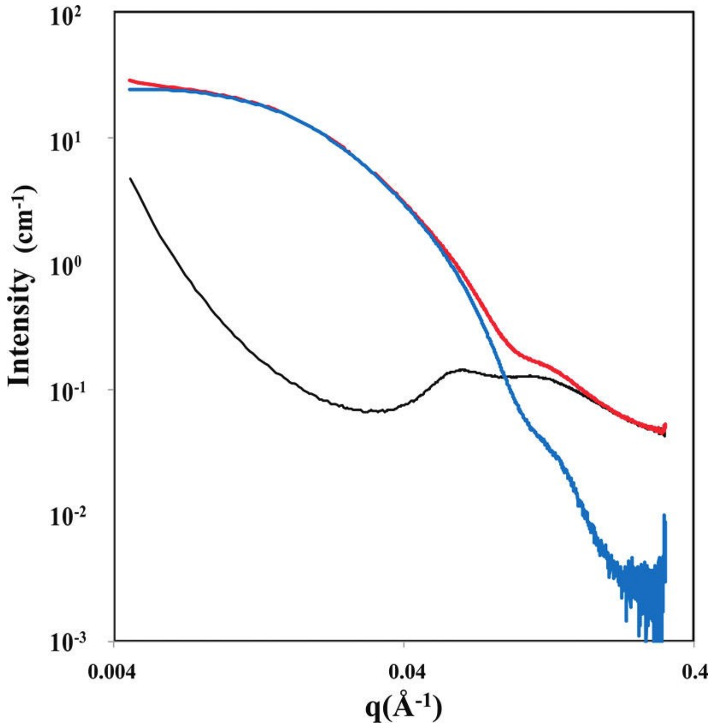

CTAB micelles in the solution

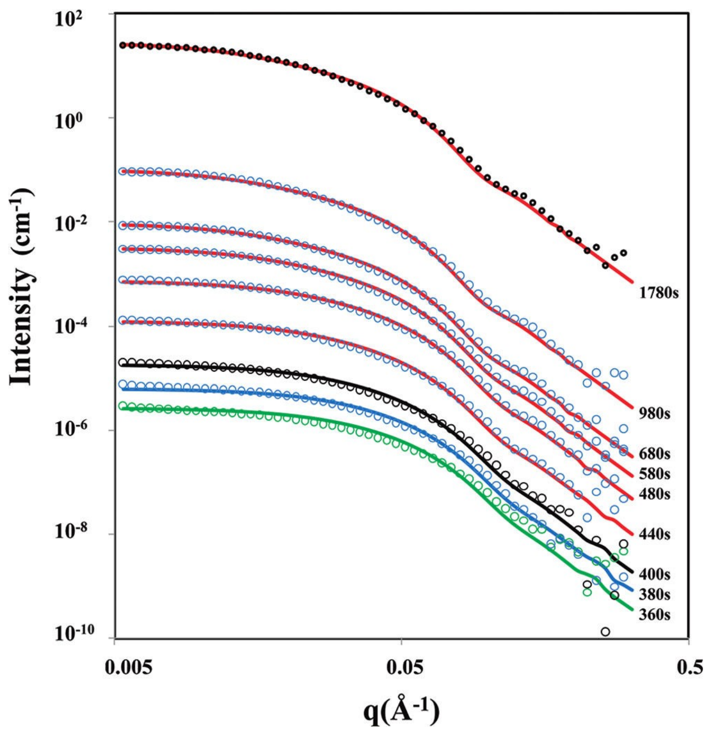

F. Hubert et al. Cryst. Growth Des. 2012

Synthesis of Gold Nanorods

SAXS allows the determination of :

- Total amount of gold in solution
- Size, shape and distribution of nanorods

Anisotropy acquired during growth phase

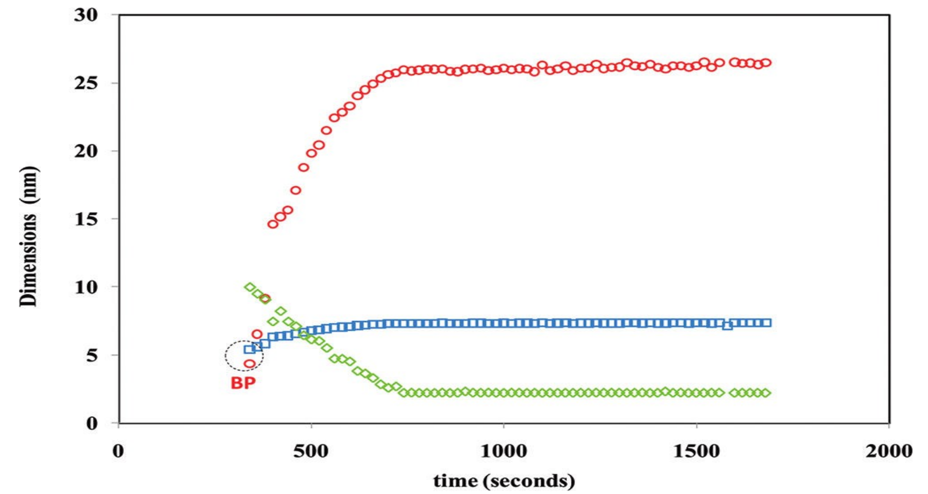

Length, diameter and length dispersion

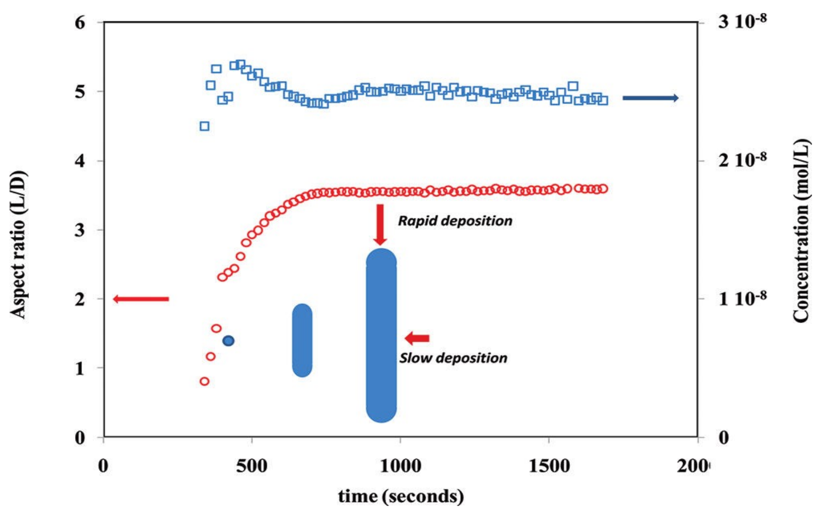

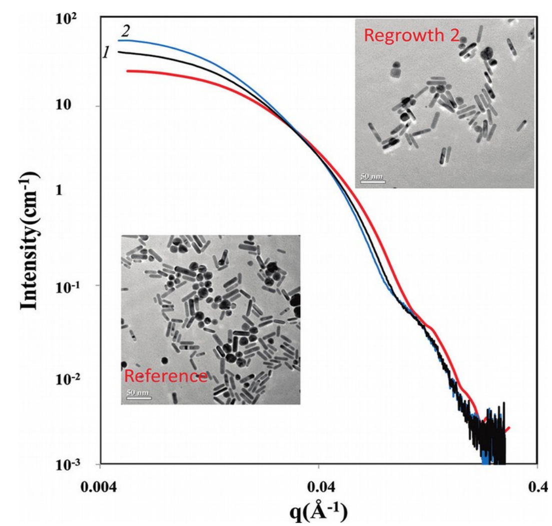

Regrowth experiment : AR increases from 3.6 to 4.4

Synthesis of Gold Nanorods

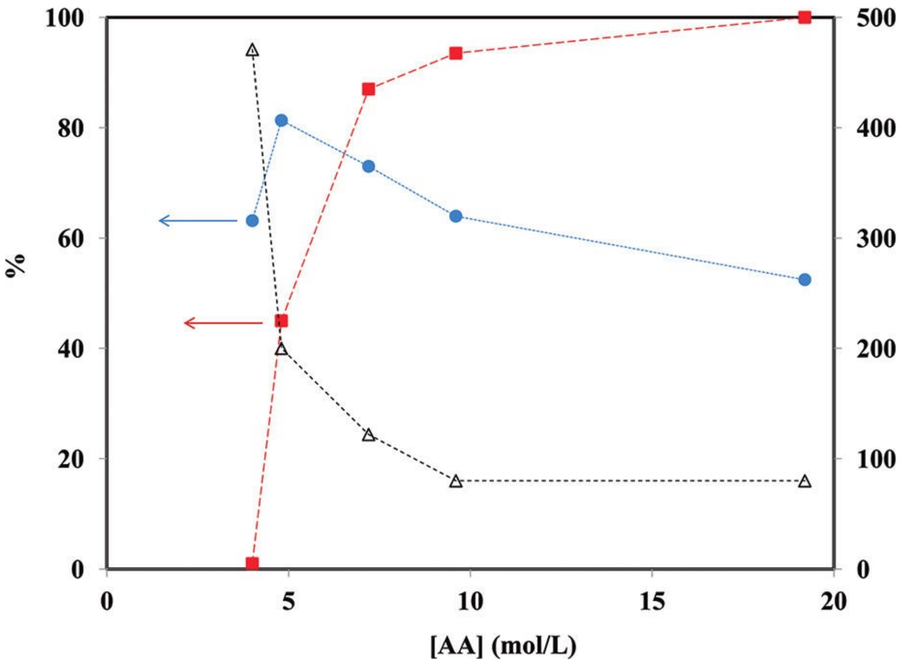

Yield, % of rods and time of reaction against ascorbic acid concentration

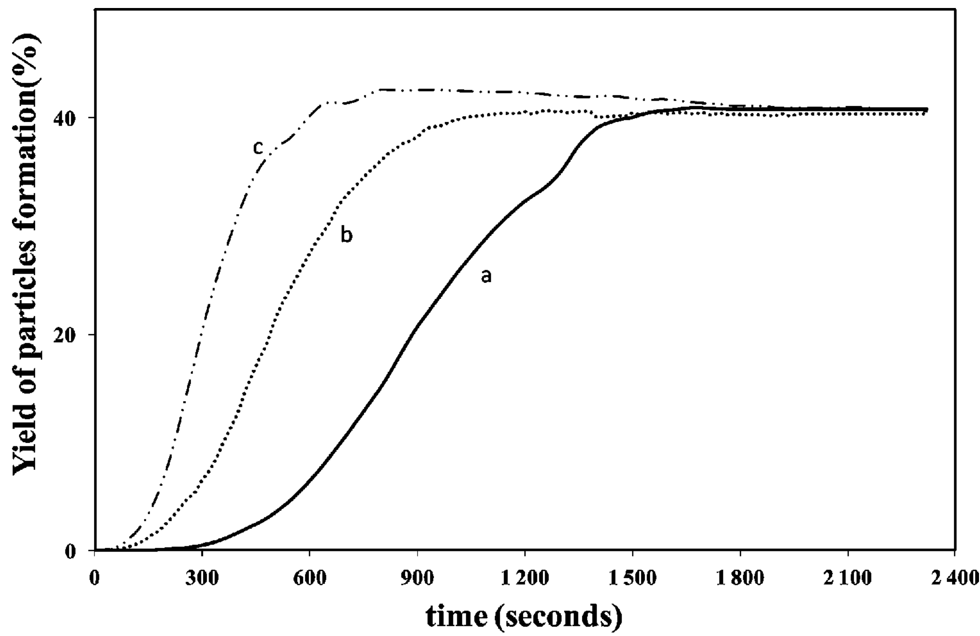

Influence of Borohydride on reaction yield

Reduction of Au(III) to Au(0) in a 2 step process
(Ascorbic acid only gives 2 electrons

Synthesis of Gold Nanorods

XANES

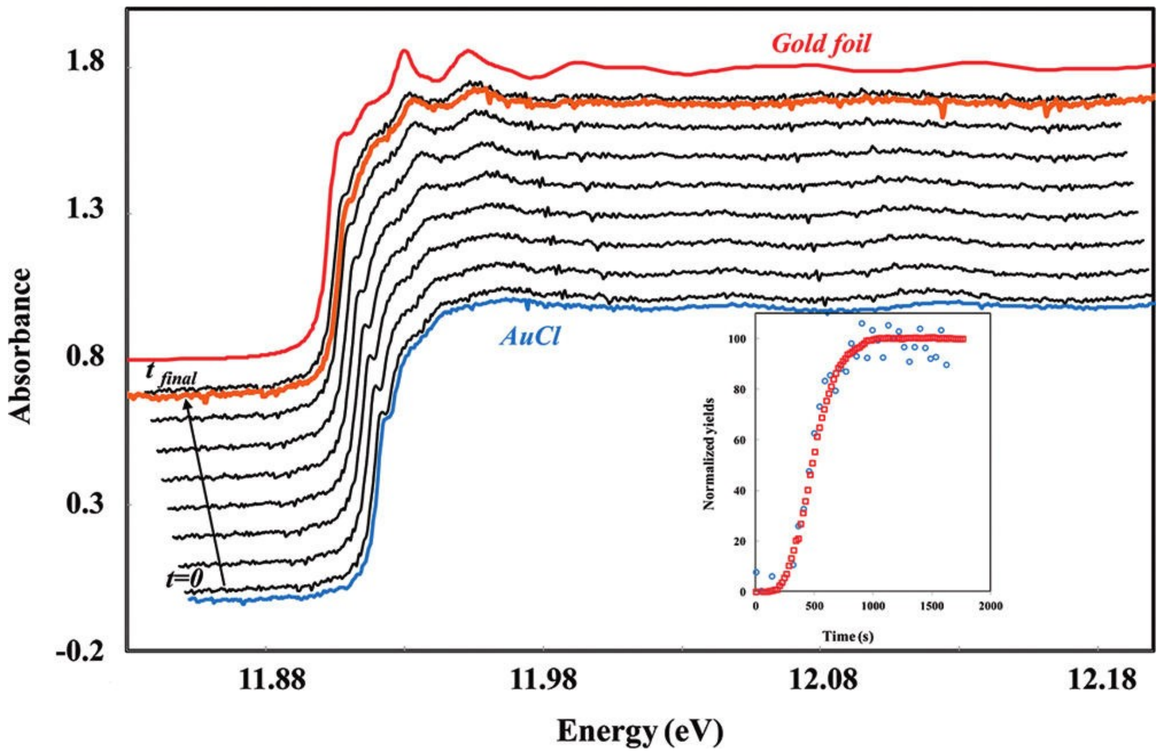

- No Au(0) in solution
- Surface reaction of Au(1) to Au(0). Surface catalyzes the oxidation of ascorbic acid

Graphene

- 6 points Fermi surface
- Dirac equation, zero mass

$$E(\delta k) = \hbar v_F \delta k$$

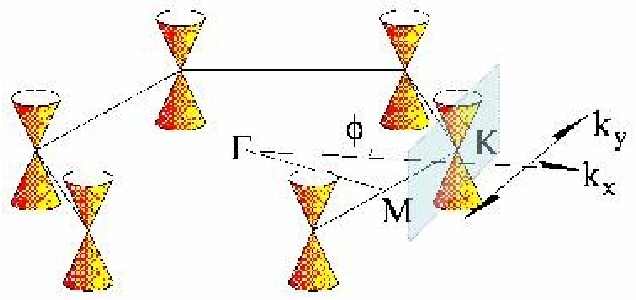

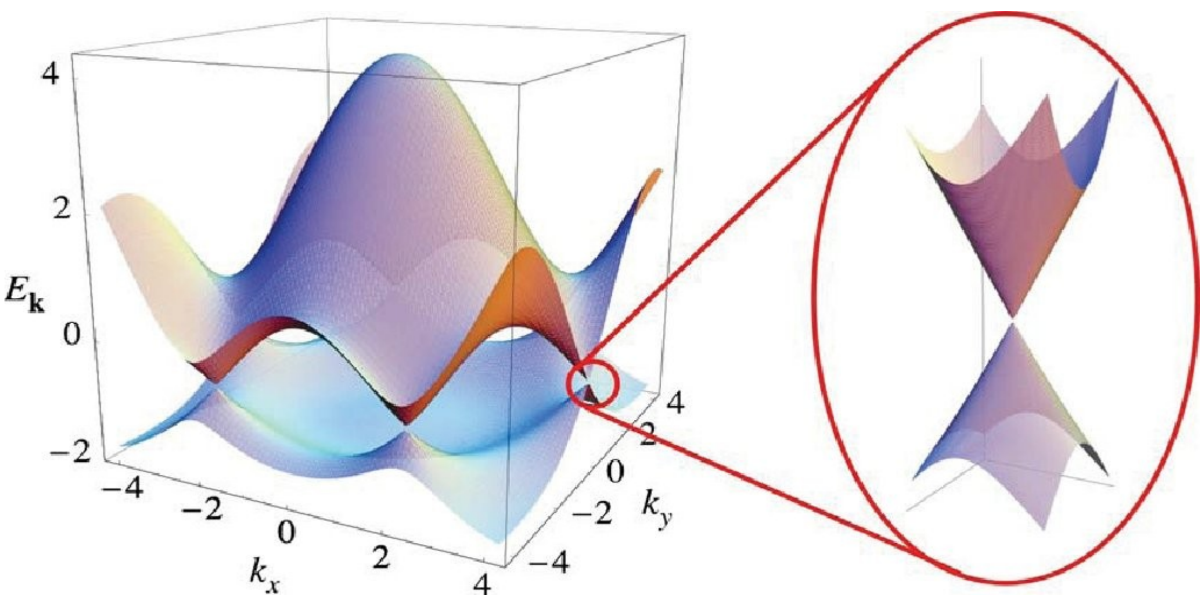

First Direct Observation of a Nearly Ideal Graphene Band Structure

Angle Resolved PhotoEmission Spectroscopy (ARPES)

M. Sprinkle *et al.*, Phys. Rev. Lett. **103** 226803 (2009)

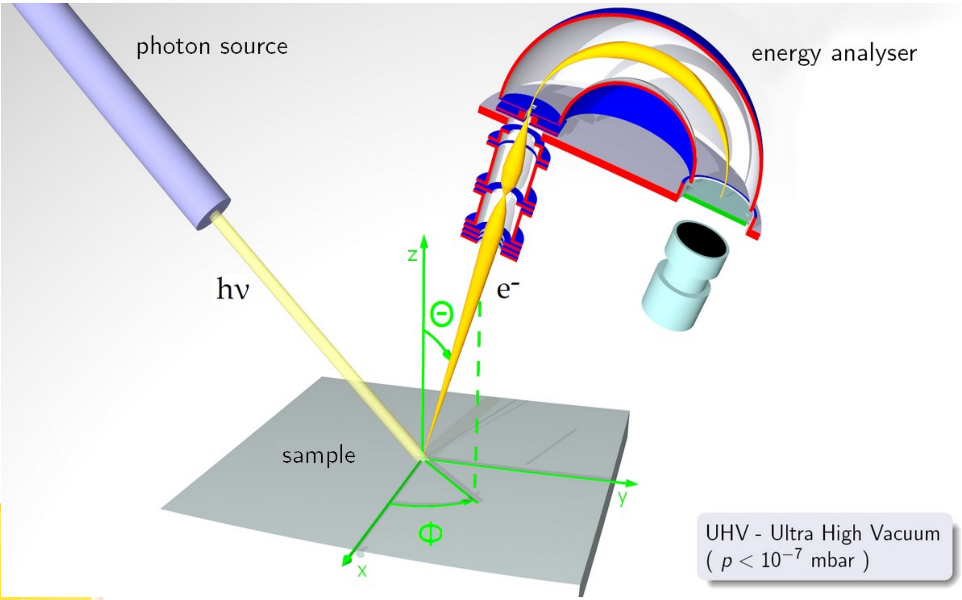

SiC $(000\bar{1})$

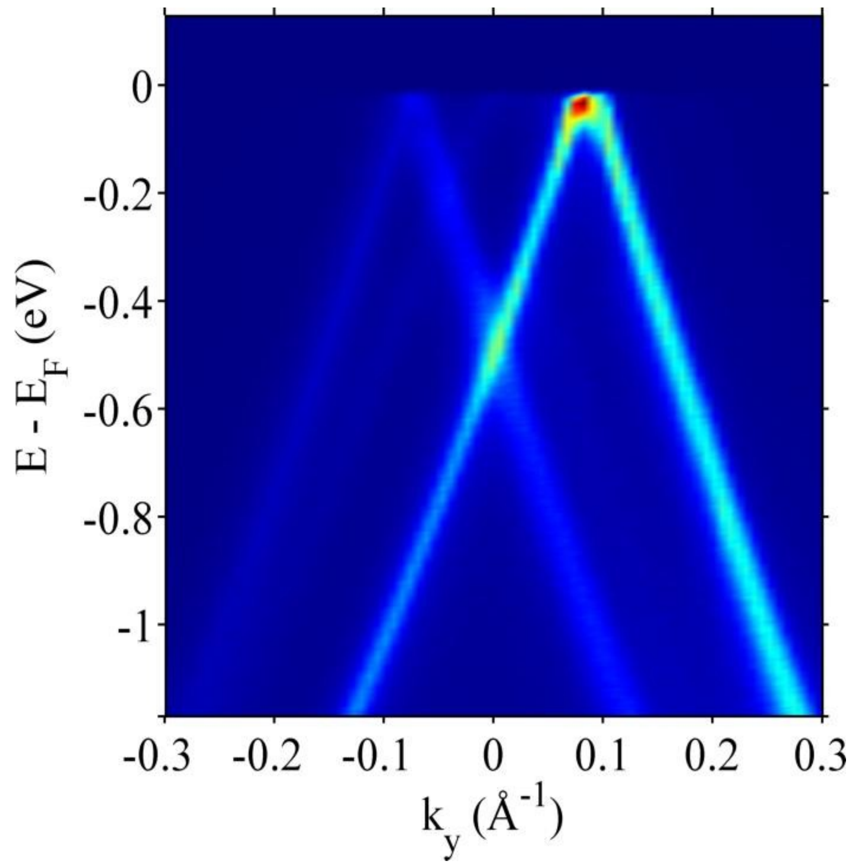

Gap opening in armchair graphene nano-ribbons

E.H. Conrad *et al.*, Georgia Tech Atlanta

Need of a gap to use graphene in electronic devices

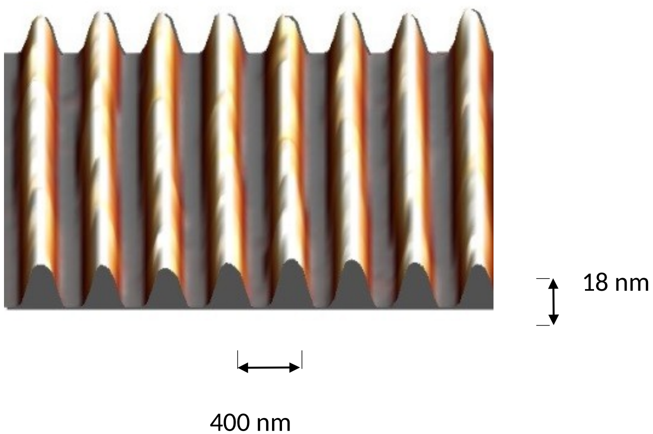

Growth of graphene on pre-patterned SiC surfaces

Control of graphene-substrate interaction

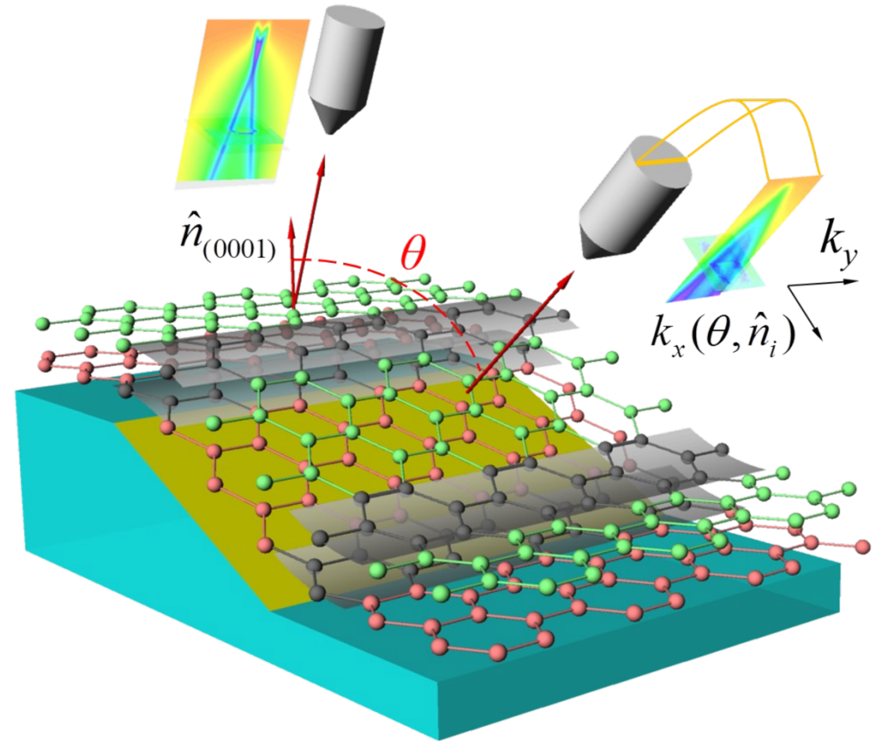

ARPES measurements performed on different areas (corresponding to different orientations by rotating the samples)

J. Hicks *et al.*, Nat. Phys. **9**, 49 (2013).

Gap opening in armchair graphene nano-ribbons

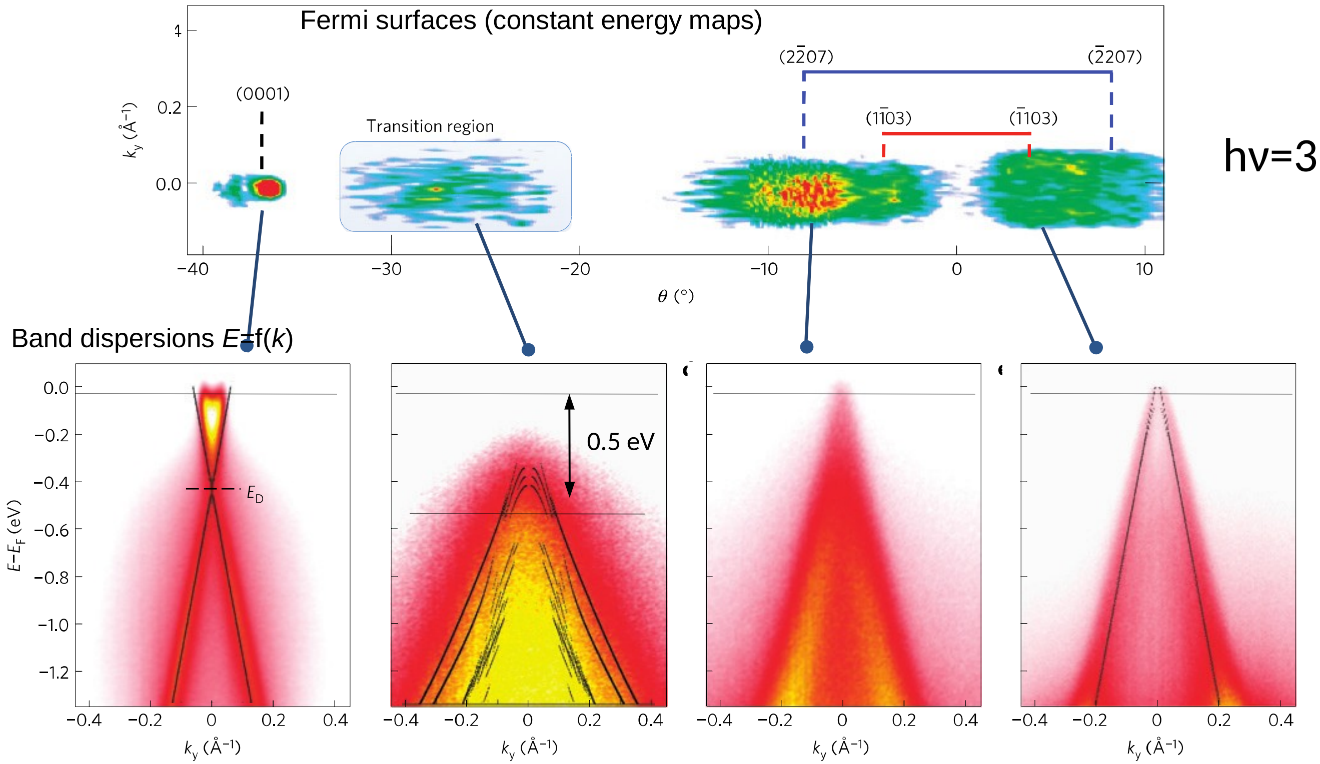

hv=36 eV

Opening of a 500 meV gap in the ~ 1.4nm wide bent graphene

flat surface

nano-ribbons (bent graphene)

facets of the sidewalls

One-dimensional metallic–semiconducting–metallic junction made entirely from graphene.

J. Hicks *et al.*, Nat. Phys. **9**, 49 (2013).

ANTARES : NanoARPES Beamline

20eV-900eV
30nm resolution
Interferometric control

- **Nano-Core Levels**
- **Nano-ARPES**
- **Nano-Photodiffraction**
- **Nano-X-ray absorption**

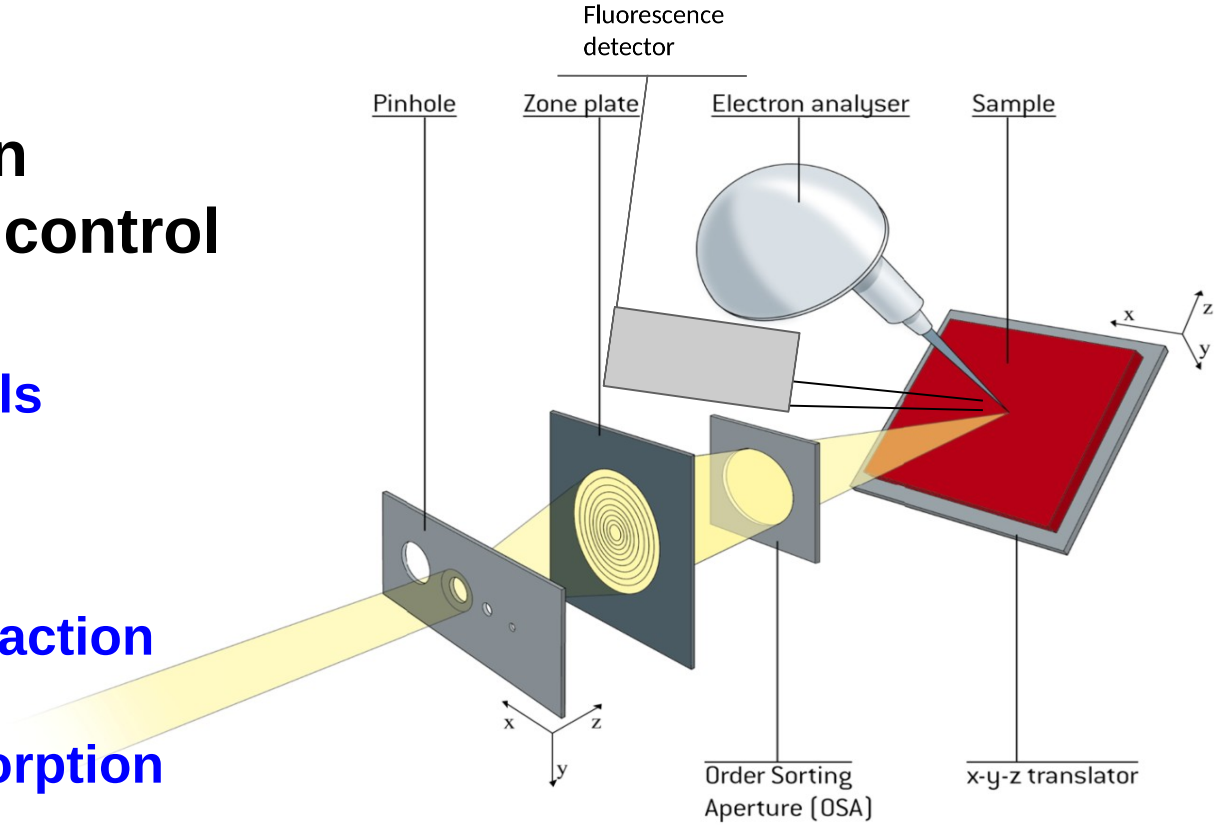

Photoelectron detection, Zone Plate focalisation and sample nano-scanning

Imaging exfoliated Graphene/SiO_2 using nanoARPES and nano-core levels

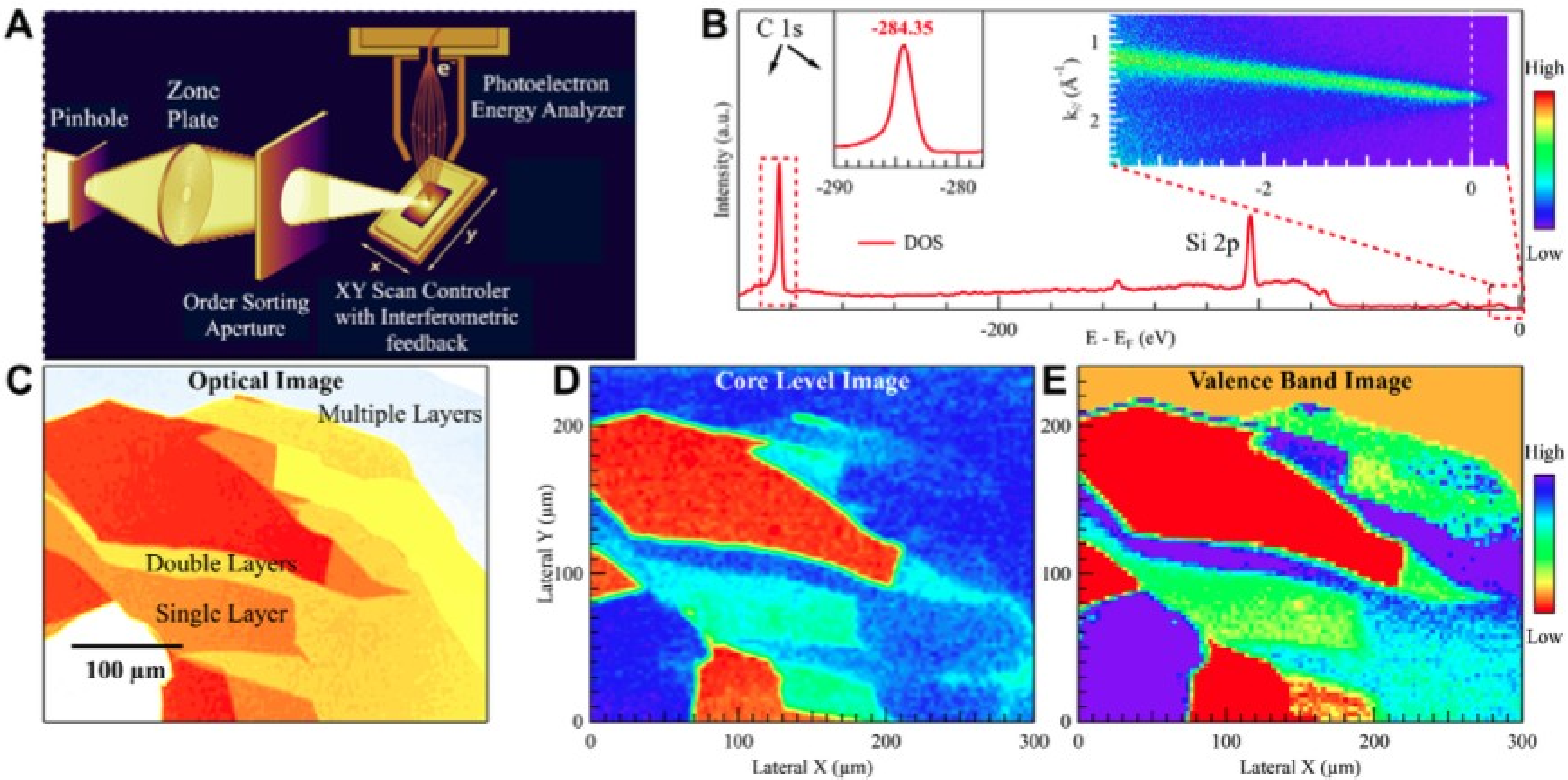

Graphene becomes visible in an optical microscope if placed on top of a Si wafer with a carefully chosen thickness of SiO_2, owing to a feeble interference-like contrast with respect to an empty wafer.

Highly Oriented Pyrolitic Graphite (HOPG)

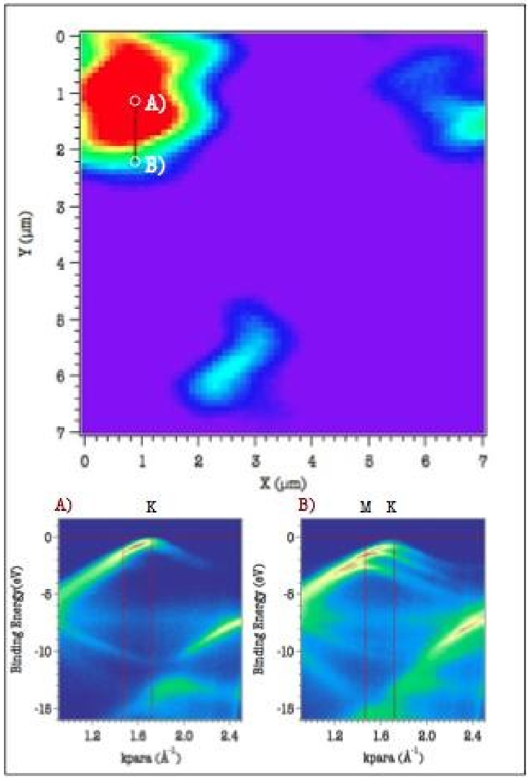

HOPG crystals are composed of µm grains

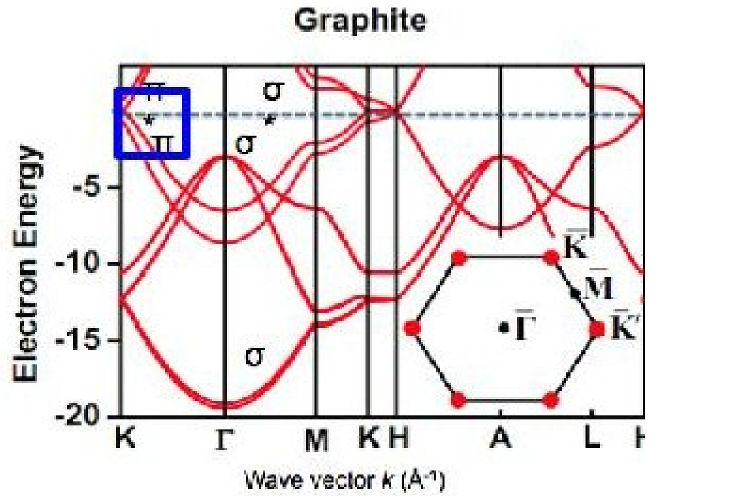

Fermi surface

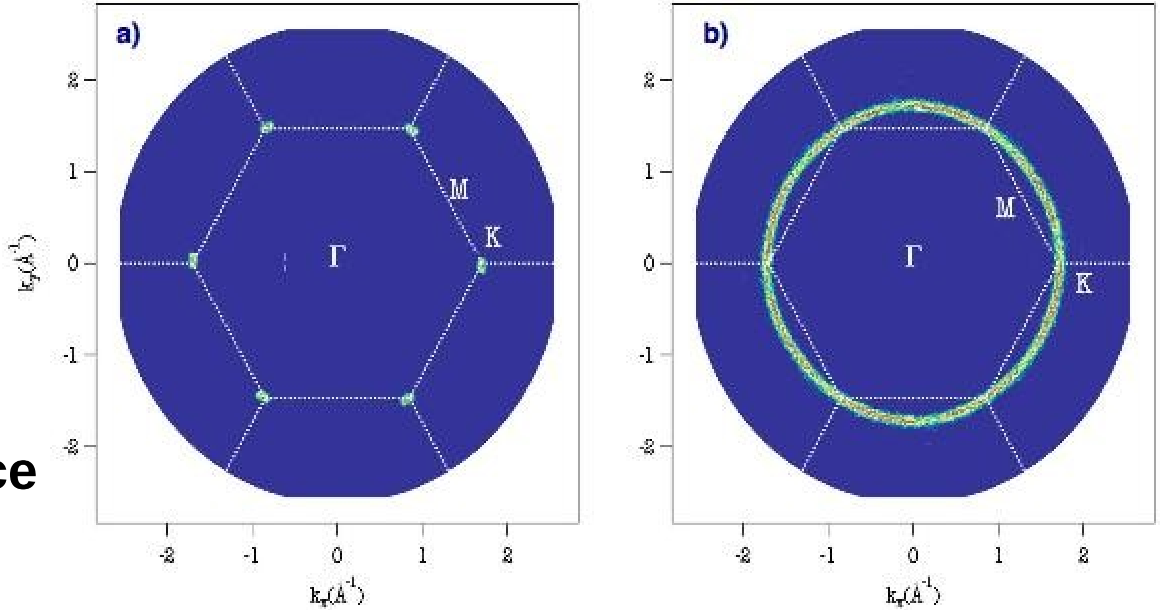

Graphene on SiC

Coll. IEMN, Lille

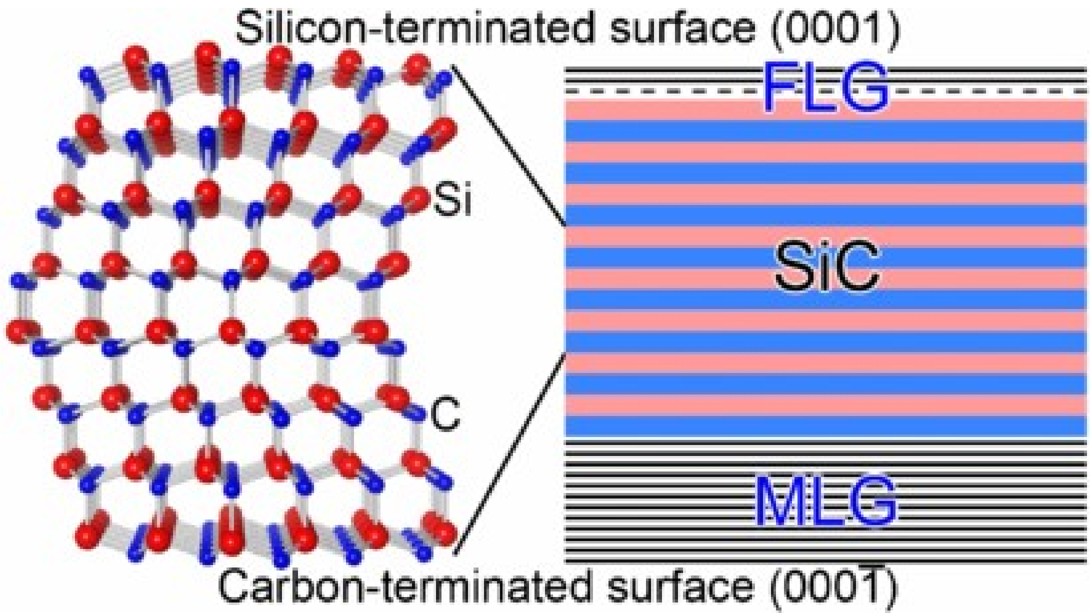

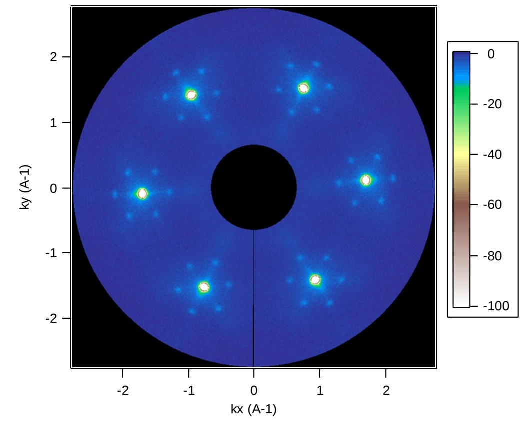

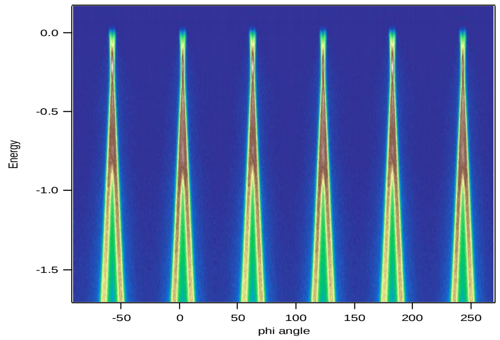

- **Si-face: only a few graphene layers (FLG) growth**
- **C-face: graphene multilayers (MLG) growth with grains**

Higher mobility

SiC (0001)

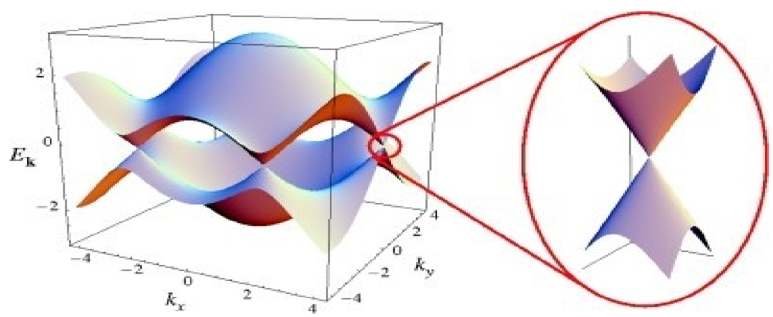

Fermi surface on SiC C-face

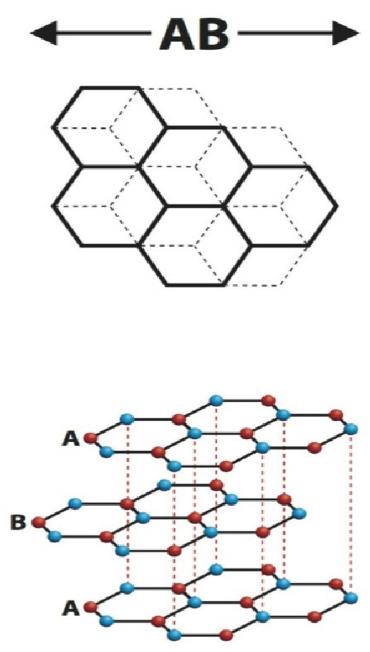

Bernal stacking

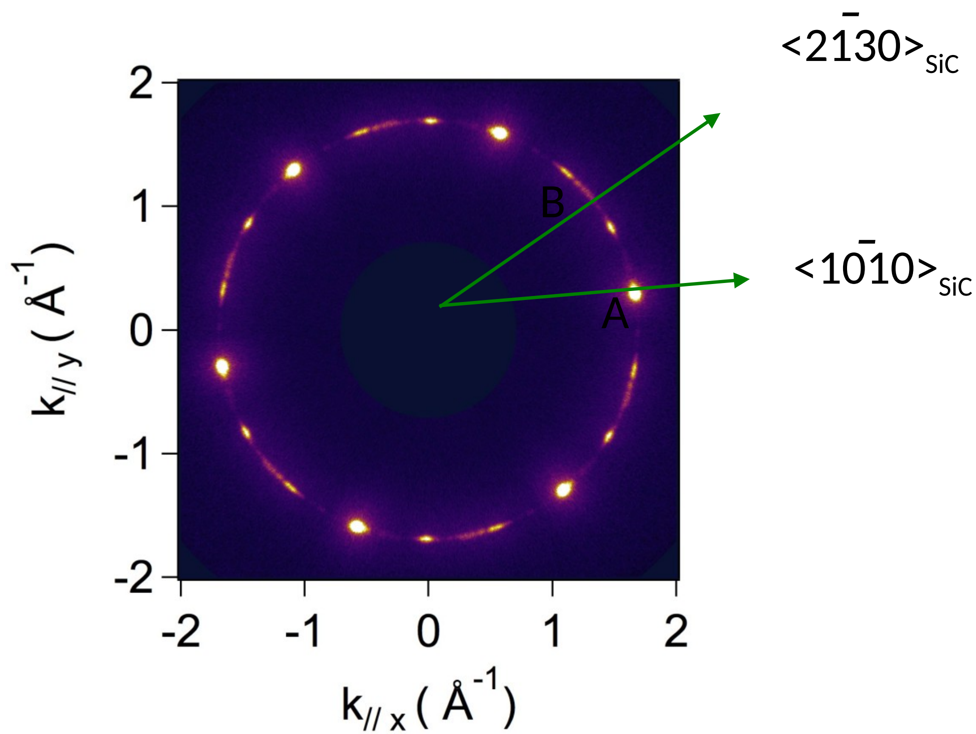

Johansson et al.,
Nature Scientific Reports
4 (2014) 4157

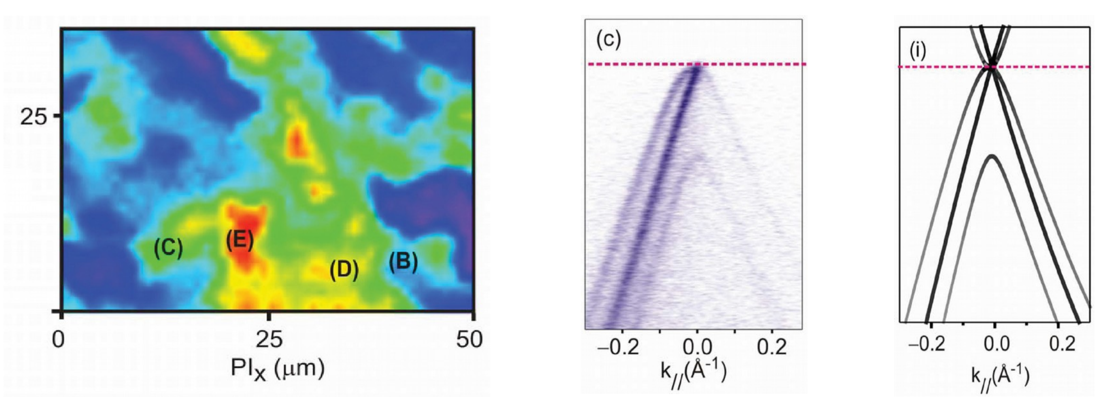

Graphene grains oriented along $\langle 10\bar{1}0 \rangle$

Si flux assisted MBE

Razado-Colombo et al., Phys. Rev. B (2015

IEMN, Antares

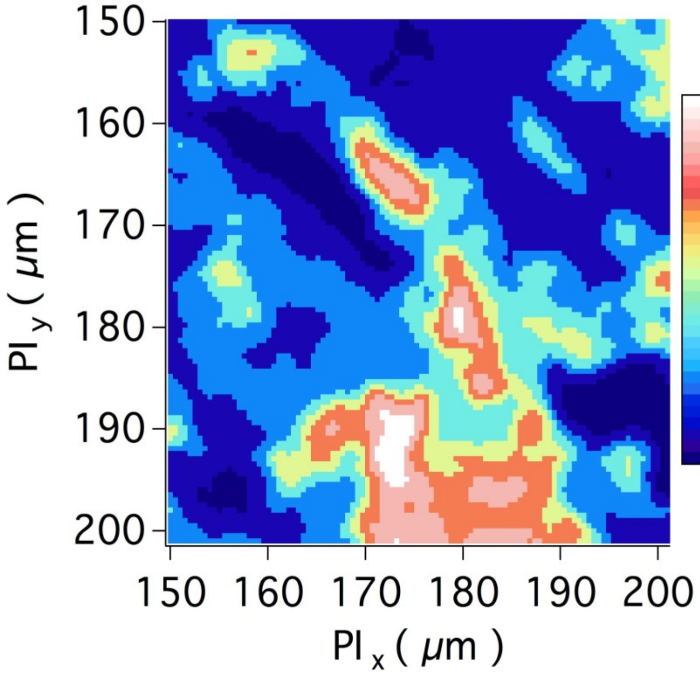

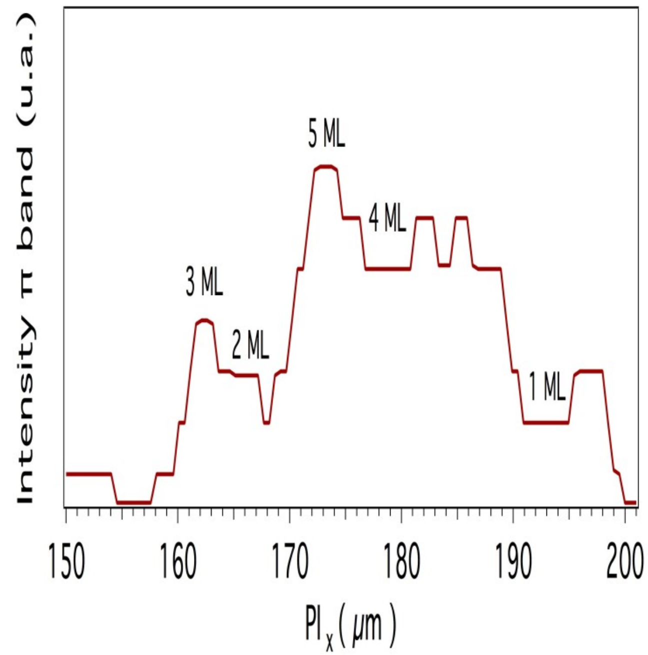

BE= 0.80 eV

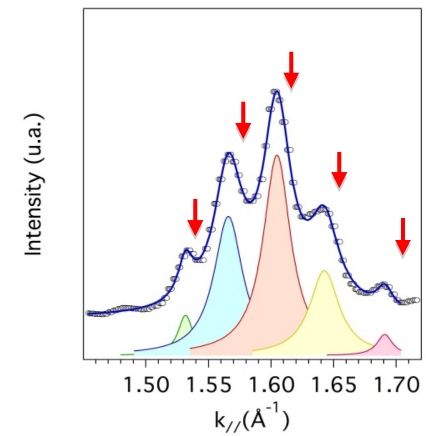

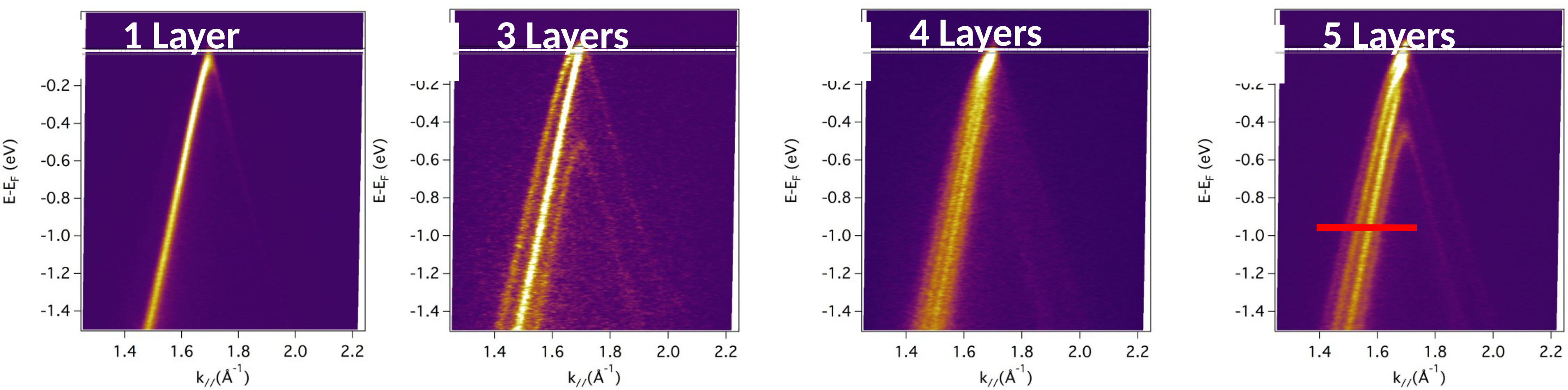

Graphene grains oriented along $\langle 21\bar{3}0 \rangle$

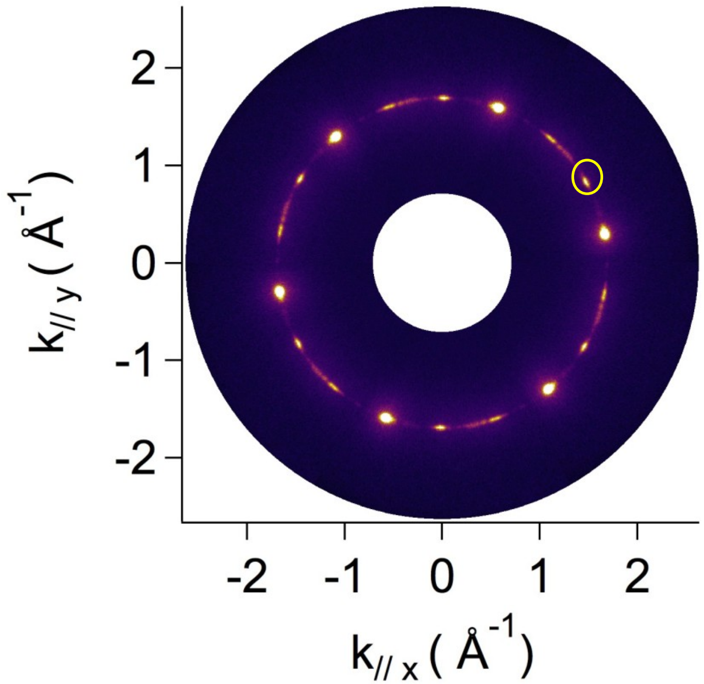

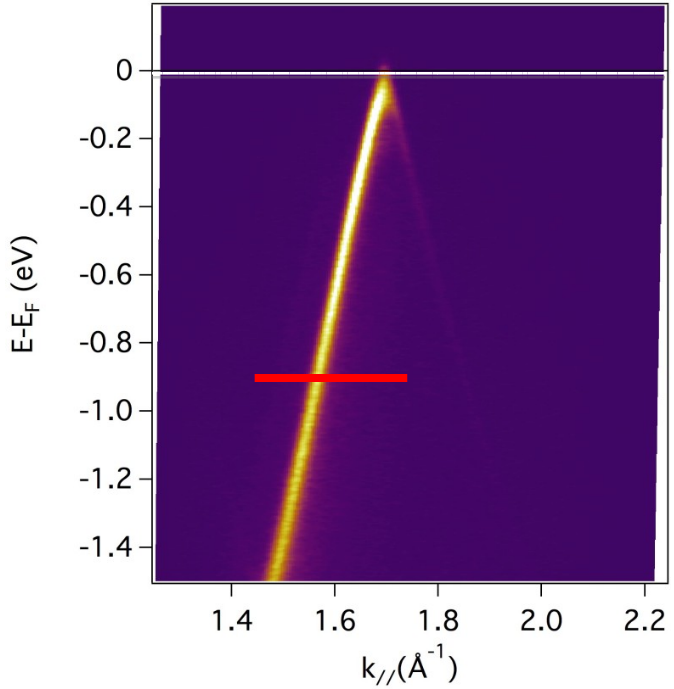

Only one band: twisted bilayer or single layer

C-face SiC $(000\bar{1})$

Intensity of the electronic states at the Fermi level as a function of x and y.

Grains oriented along the step edges or <10-10> directions grow as multilayer graphene films.

Grains oriented along the two equivalent <21-30> directions provide only monolayer and bilayers graphene films.

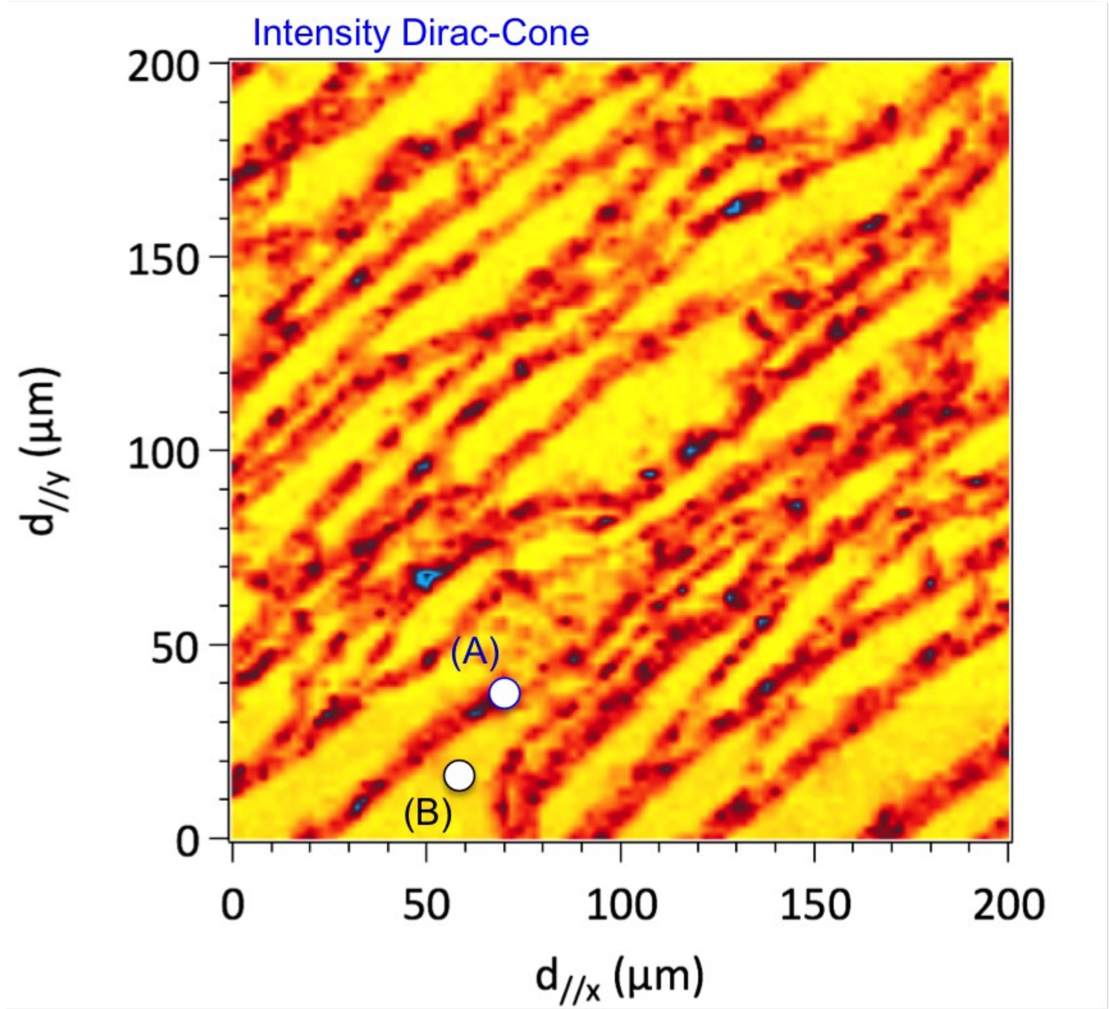

Coherence of the Beam

Synchrotron beams are partially coherent

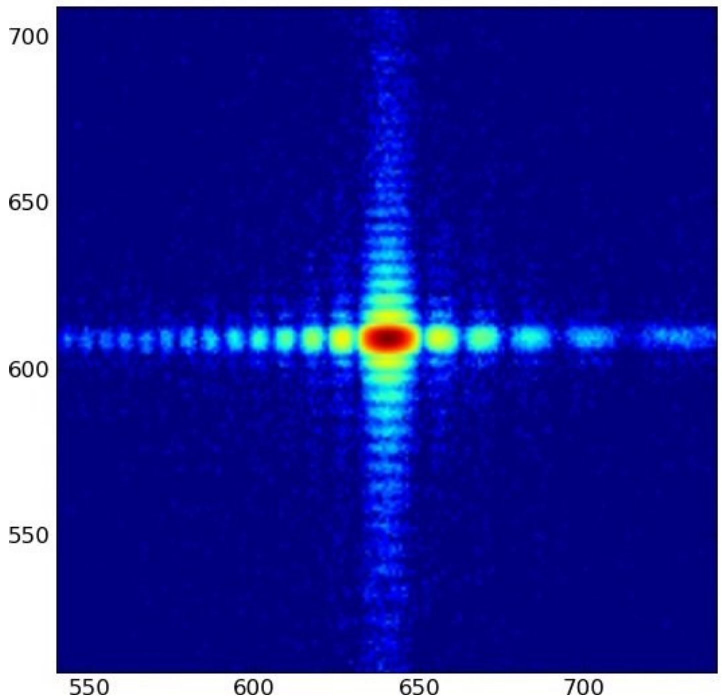

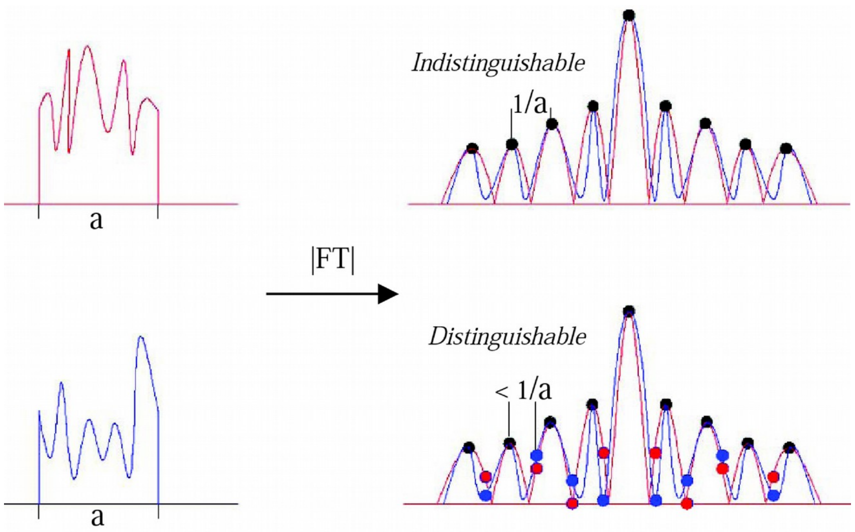

After J. Miao

Phase problem, Oversampling

Constraints on support
Reconstruction algorithms

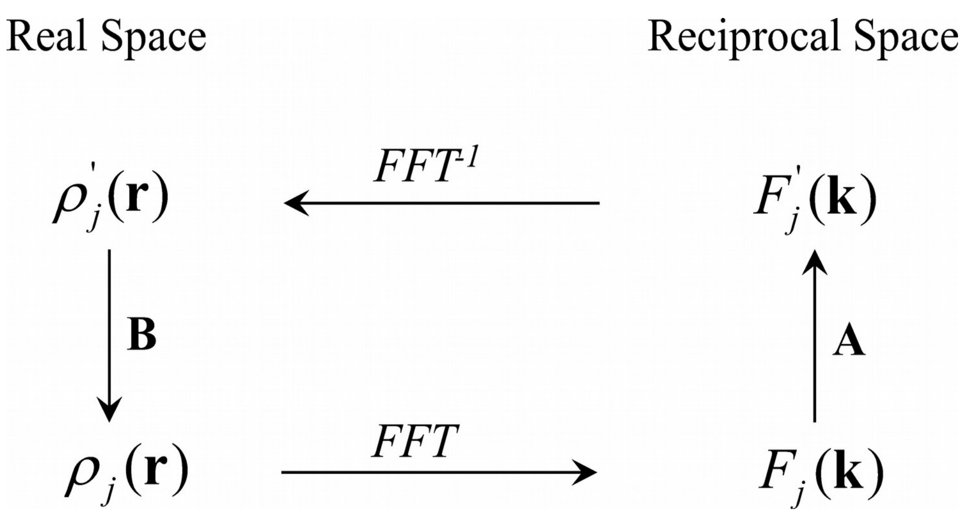

Trace Elemental Imaging of Fossils

Interpretation of flattened fossils difficult

- Late cretaceous shrimp and fish
- Fossilization is a complex process
- Fluorescence mapping of rare-earth elements helps in identifying skeletal elements
- Statistical analysis of full spectra

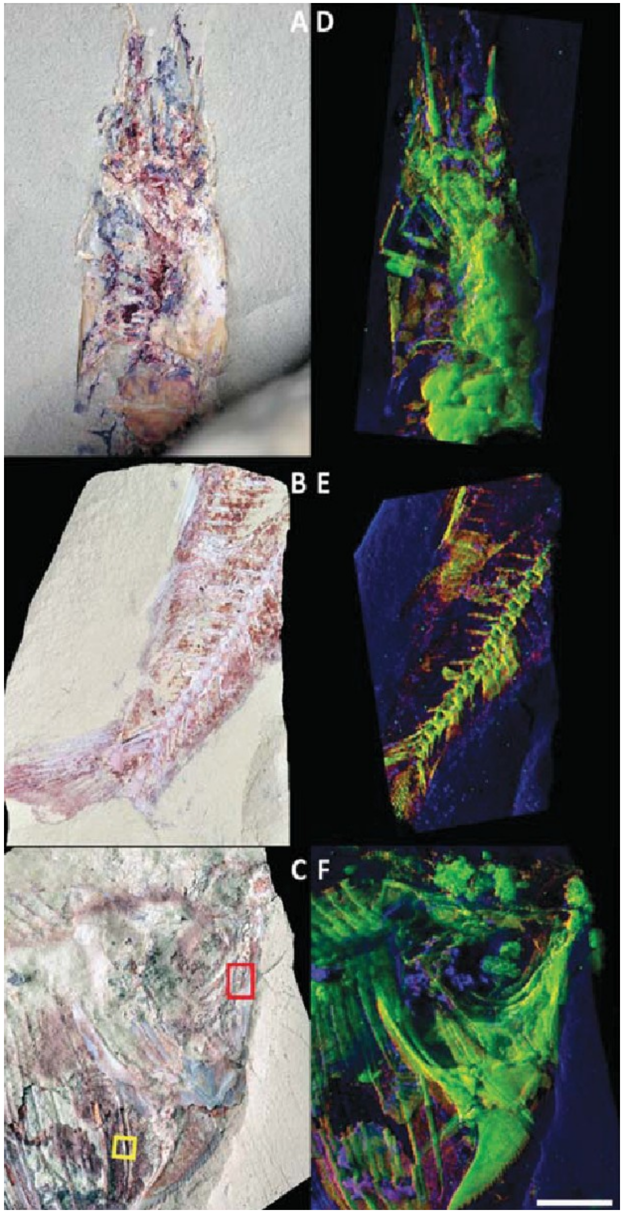

5 mm

Gueriau et al., PlosOne 2014

Free Electron Lasers

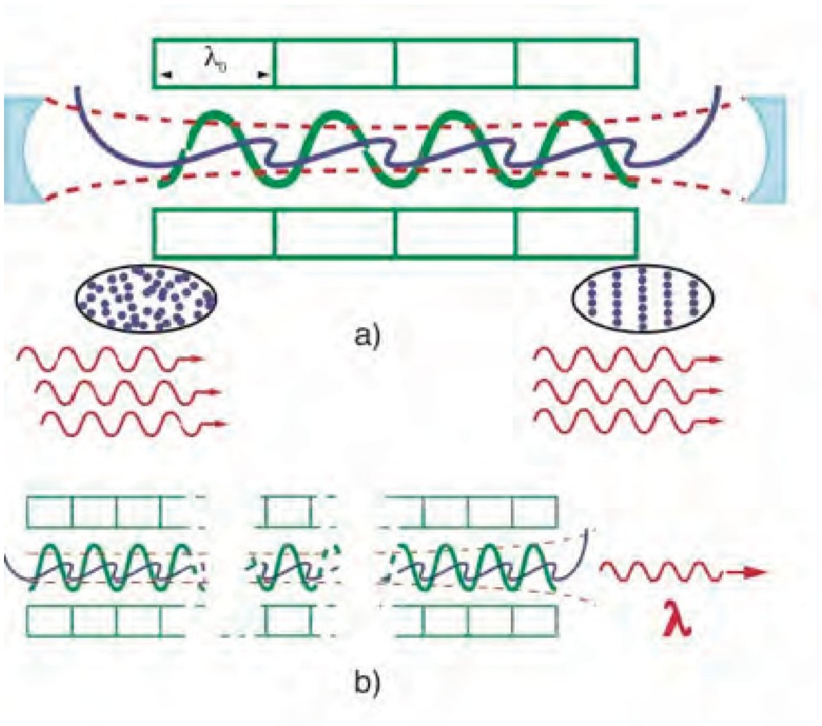

Linac Coherent Light Source (LCLS)
Stanford, Ca

Free Electron Lasers

Ring opening of cyclohexadiene

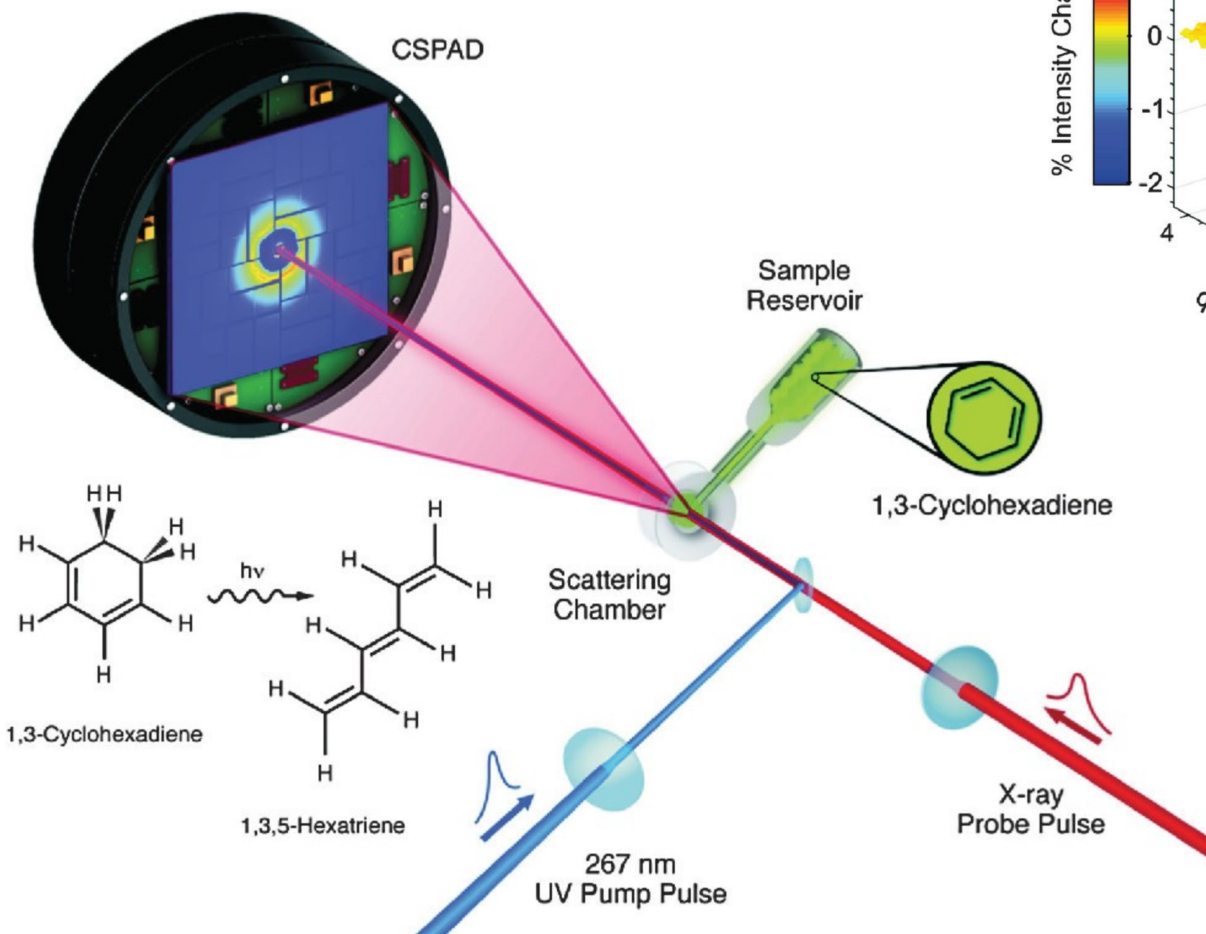

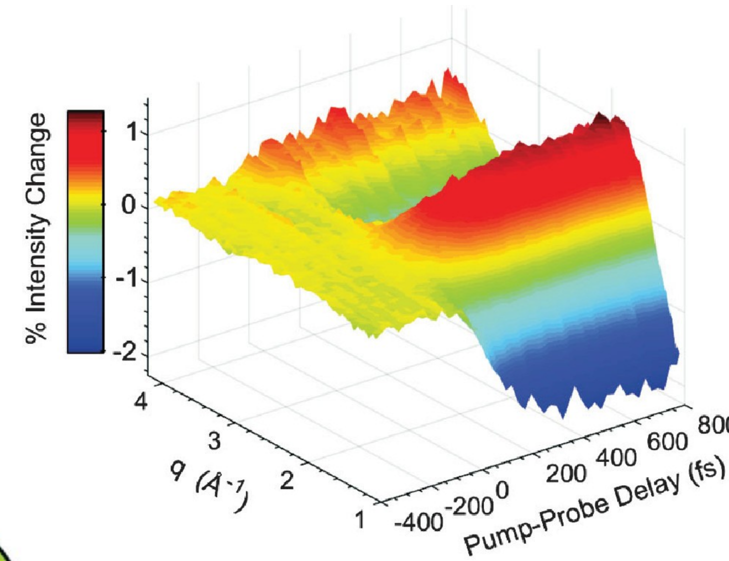

Minitti et al., Phys. Rev. Lett. 2015

Thank you!

F. Sirotti, P. Lagarde, M.-C. Ascencio, E. Elkaim, A. Coati, P. Fontaine, D. Thiaudière, E. Otero, P.Ohresser, H. Tissot, R. Belkhou